Journal of Inorganic Biochemistry 269 (2025) 112882

Contents lists available at ScienceDirect

Journal of Inorganic Biochemistry

journal homepage: www.elsevier.com/locate/jinorgbio

Synthesis, crystal structure, computational and solution studies of a new phosphotetradecavanadate salt. Assessment of its effect on U87 glioblastoma cells

Rim Zarroug [a,b,***], Wassim Moslah [c], Najet Srairi-Abid [c], Beñat Artetxe [d], Albert Masip-Sánchez [e], Xavier López [e,**], Brahim Ayed [a], Nádia Ribeiro [f], Isabel Correia [f], Leonor Corte-Real [f], João Costa Pessoa [f,*]

[a] University of Monastir, Laboratory of Physico-Chemistry of Materials LR01ES19, Faculty of Sciences of Monastir, Tunisia
[b] Department of Chemistry, Faculty of Sciences, University of Gabes, Tunisia
[c] Université Tunis El Manar, Institut Pasteur de Tunis, LR20IPT01 Biomolécules, Venins et Applications théranostiques (LBVAT), 1002 Tunis, Tunisia
[d] Departamento de Química Orgánica e Inorgánica, Facultad de Ciencia y Tecnología, Universidad del País Vasco UPV/EHU, 48080 Bilbao, Spain
[e] Universitat Rovira i Virgili, Departament de Química Física i Inorgànica, c/Marcel·lí Domingo 1, 43007 Tarragona, Spain
[f] Centro de Química Estrutural and Departamento de Engenharia Química, Institute of Molecular Sciences, Instituto Superior Técnico, Av. Rovisco Pais, 1049-001 Lisboa, Portugal

ARTICLE INFO

Keywords:
Polyoxidometalates
X-ray diffraction
Density functional theory
Molecular dynamics calculations
Anti-cancer activity
Glioblastoma

ABSTRACT

The new benzylammonium ($C_7H_{10}N$) salt of the phosphotetradecavanadate (PV14) anion $PV_{14}O_{42}^{9-}$, $(C_7H_{10}N)_6[H_3PV_{14}O_{42}]\bullet 7H_2O$ (1), is synthesized under mild conditions and characterized by a combination of physicochemical techniques such as Fourier transform infrared spectroscopy, powder X-ray diffraction, elemental analyses and cyclic voltammetry. As evaluated by ^{51}V NMR spectroscopy, at milimolar concentrations and pH ~2.5 the PV14 anions decompose slowly, thus demonstrating kinetic stability, but at pH ~7 this process takes place much faster. However, in the presence of human serum albumin, the ^{51}V NMR peaks of PV14 anions broaden significantly and their decomposition becomes much slower, this being due to a direct interaction between both components. The structure of **1** is elucidated by single-crystal X-ray diffraction and reveals the presence of three-fold protonated, bicapped Keggin type $[H_3PV_{14}O_{42}]^{6-}$ anions. The supramolecular interactions governing the crystal packing are further studied using the Hirshfeld surface analysis. Computational studies using density functional theory were effective in determining the electronic and protonation states of PV14 clusters, as well as the multi-electron redox behavior of compound **1** in acidic aqueous solutions. Molecular dynamics calculations confirm the high hydrophilicity and absence of aggregation between protonated PV14 anions in aqueous medium. Notably, this compound shows high inhibitory effect on the viability of the U87 glioblastoma cell line with IC_{50} values of 3.2 ± 0.6 μM and 1.10 ± 0.04 μM after 24 h and 72 h treatments. The mode of action of compound **1** is mediated by the pro-apoptotic process. These data provide evidence on the potential therapeutic use of PV14 compounds against glioblastoma.

Abbreviations: BSA, Bovine serum albumin; BVS, Bond Valence Sum calculations; CV, cyclic voltammetry; *de*, distance from the point to the nearest nucleus external to the surface; *di*, distance to the nearest nucleus internal to the surface; DFT, Density Functional Theory; *dnorm*, normalized contact distance; δ_V, ^{51}V NMR chemical shift; HS, Hirshfeld surface; HSA, human serum albumin; Hepes, 4-(2-hydroxyethyl)-1-piperazineethanesulfonic acid; LHR, luteinizing hormone receptor; PE, protonation energy; POM, Polyoxidometalate; POV, Polyoxidovanadate; PV14, phosphotetradecavanadate; SC-XRD, single-crystal X-Ray diffraction; V1, monovanadate; V2, divanadate; V4, tetravanadate; V10, decavanadate; vdW, van der Waals radii.

* Corresponding authors.
** Corresponding author.
*** Corresponding author at: University of Monastir, Laboratory of Physico-Chemistry of Materials LR01ES19, Faculty of Sciences of Monastir, Tunisia.
E-mail address: joao.pessoa@ist.utl.pt (J.C. Pessoa).

https://doi.org/10.1016/j.jinorgbio.2025.112882
Received 29 January 2025; Received in revised form 25 February 2025; Accepted 3 March 2025
Available online 9 March 2025

1. Introduction

Polyoxidometalates (POMs) constitute a class of inorganic anions made of discrete polymetallic oxide frameworks based mainly on high valence transition metals such as W^{VI}, Mo^{VI} or V^{V} [1–3]. The simple general formula $[M_xO_y]^{n-}$ covers a large structural diversity and a wide range of reactive and modifiable structures [4–7], with diverse applications in the field of chemical engineering [8] but also in many other areas, such as catalysis [9–12], environmental science [13], materials science [14–20], biochemistry, pharmacology, medicine [4,5,7] and energy-storage applications [20–26].

Several research groups have tested different vanadium compounds (VCs) to find new potential drugs [27–38]. In fact, VCs have been shown to display important biological effects, which suggest their potential both in fundamental and clinical applications. VCs are especially interesting compounds because of the variable and easily accessible oxidation states that vanadium can adopt (V^{III}, V^{IV} and V^{V}), as well as diverse nuclearity, coordination modes and geometries [37]. In contrast to W and Mo, the different nuclearities and coordination polyhedra displayed by vanadium based POMs further justify the research on this family of compounds [39–43].

Vanadate ions and vanadium compounds may stimulate or inhibit the activity of enzymes, most of these effects being attributed to the similarities of vanadate(V) anions with phosphate(V) [28,37,44–50]. Noteworthy, polyoxidovanadates (POVs) have been reported to have ion pumps, such as Na^+/K^+-ATPase and Ca^{2+}-ATPase, among the possible targets in their biological action [45,51–55]. Several other types of biological effects have been attributed to POVs [29,54,56–61]; for instance, studies have shown that VCs and POVs can interfere on different aspects of the cancerogenesis, such as cell proliferation and viability [29,60,62–67].

Glioblastoma is a very aggressive type of brain cancer (glioma) affecting the central nervous system, that accounts for a high proportion of malignant brain and nervous system tumors [68–70]. Presently, the treatment of glioblastoma is based on chemotherapy with temozolomide (TMZ) [71–76]. However, resistance to TMZ has limited the efficiency of this drug [72–75,77], so there is a need to develop therapies that can induce cell death through alternative pathways.

Among VCs reported to have effect on glioblastoma cells we can cite $V^{V}O_2(L^1H)$ (L^1H_2 = 2-hydroxy-1-naphthylaldehyde isonicotinoyhydrazone), where both the complex and the free ligand were active against human glioblastoma T98G cancer cells [78] The compound $V^{IV}O(acac)_2$ (Hacac = acetylacetone) was also reported to suppress glioblastoma cells' growth, with IC_{50} values in the range 4–6 μM, showing low toxicity to major neural cells and not inducing immunogenic responses [79]. Interestingly, it was also found that using graphene oxide quantum dots as route of administration, the efficacy was significantly increased and the toxicity was reduced. More recently Crans and co-workers [80], using viability assays, evaluated and compared the anti-proliferative activity of several related vanadium mixed-ligand complexes containing Schiff bases- and catechol-type ligands in T98G glioblastoma and SVG p12 normal glial cells. Most of the compounds tested form non-toxic by products upon degradation. The better properties of [VO(3-tBuHSHED)(TIPCAT)] (3-tBuHSHED = N-(3-tert-butyl-salicylideneaminato)-N-(2-hydroxyethyl)-1,2-ethanediamine and TIPCAT = 3,4,6-tri-isopropylcatechol) compared to others tested were attributed to the greater steric hindrance associated to the new 3-tBuHSHED and catecholato (TIPCAT) ligands. Besides emphasizing the need to mitigate adverse effects from possible metabolites, the authors also discussed the relevance of the hydrophobic properties for the enhancement of the cytotoxicity and in improving the aqueous stability of the complexes within the tumor microenvironment.

These previous studies on finding suitable VCs and formulations for the efficient delivery of vanadium compounds [37] has been encouraging the development of new VCs for the treatment of glioblastoma as well as other types of malignant tumor cells. In fact, efficient cellular uptake is important for the efficacy and potency of vanadium-based drugs [37,81–85] and subtle modifications in their structures may be relevant for faster uptake and to enhance their specificity [62,84]. The luteinizing hormone receptor (LHR) is expressed in Chinese Hampster Ovary (CHO) cells and was reported to initiate signaling in the presence of some POVs, for example with the decavanadate $Na_3[H_3V_{10}O_{28}]$ (**2**) and with the mixed-valence phosphotetradecavanadate $K(NH_4)_4[H_6V_{14}O_{38}(PO_4)]$ (**3**) [62] (phosphotetradecavanadates will be abbreviated as PV14). In this particular study, it was reported that interactions of vanadium compounds with CHO cells decrease the packing of membrane lipids, drive aggregation of LHR and increase signal transduction by LHR. The growth inhibition by these VCs was tested, namely with $NaV^{V}O_3$ (V1), the decavanadate (**2**), the PV14 (**3**) and a V15 compound ($[(CH_3)_4N]_6[V_{15}O_{36}(Cl)]$) (**4**). Note that both these specific PV14 and V15 compounds are mixed-valence POVs. However, most POVs get partially hydrolyzed during the experiments [86,87], thus lowering their original concentrations. The growth effects of the VCs were measured and remarkably were quite effective, as in the case of the mixed-valence PV14 tested [62]. The authors reported that all POVs tested initiated signaling, V10 and V15 showing the greatest effects on cell function, while $NaV^{V}O_3$ was significantly less active. Interestingly, the PV14 compound tested, although decomposing fast in the cell medium, displayed a significant activity. This suggested that the signaling with these POVs is quite fast, presumably acting through electron transfer processes [62]. A PV14 compound was also reported [88] to display good ex-vivo inhibiting activity on Na^+/K^+-ATPase and in vitro inhibitory effects on the Ca^{2+}-ATPase.

Glioblastoma is difficult to treat, but these examples show that some decavanadates are active towards human malignant glioma cells [63,89–91]. Encouraged by the above-mentioned studies, which demonstrated the interesting biological effects of PV14 compounds, we propose to explore POV-based compounds that can potentially feature suitable properties against glioblastoma cells. Phosphotetradecavanadates(V) (or bicapped α-Keggin type $[P^{V}V^{V}_{14}O_{42}]^{9-}$, PV14), are examples of structures containing phosphate as an internal hetero group. These compounds may be synthesized by the condensation of simple inorganic $V^{V}O_4^{3-}$ anions in acidic aqueous media in the presence of phosphate salts [86,87,92,93]. Herein, we report the synthesis of the organic-inorganic hybrid salt $(C_7H_{10}N)_6[H_3P^{V}V^{V}_{14}O_{42}]\bullet 7H_2O$ (**1**) ($C_7H_{10}N^+$ = benzylammonium cation) and its characterization by single-crystal X-ray diffraction (SC-XRD). Additionally, its electronic properties are disclosed by density functional theory (DFT) calculations and its solution behavior studied by UV–Vis and ^{51}V NMR experiments and modelled by molecular dynamics (MD) simulations.

It has been reported that organic cations may improve the bioactivity and bio-specificity of V10 compounds, making them more effective against tumors [61,94]. It has also been suggested that these cations may bind to decavanadate clusters, this allegedly facilitating the interactions of V10 with cell membranes and their uptake, as well as leading to improved anti-tumor activity. It has also been stated that organic cations can help stabilize V10 compounds under biological conditions, improving their efficacy via intra-tumor injections. We believe that organic cations may be involved in quite strong interactions with V10 or other POV anions in the solid state, but extrapolation of this to biological conditions when POVs are present at low concentrations and in the presence of relatively high concentrations of several types of cations and of potential ligands for vanadium is mainly speculation, although it may be correct in some particular cases. Additionally, the cytotoxicity of the (organic cation)-POV compound tested may be mainly or partly due to the organic compound, and this should always be checked. In this work, we investigate the effect of compound **1** on the viability of U87 glioblastoma cells, as well as that of benzylamine, to check if the observed cytotoxicity is supported by the PV14 counter ions of compound **1**. Some experiments were also done with $(NH_4)_6[H_3PV_{14}O_{42}]\bullet 19H_2O$ (**5**), a PV14 compound not containing organic cations as counter ions.

2. Results and discussion

2.1. Characterization of $(C_7H_{10}N)_6[H_3PV_{14}O_{42}]\bullet 7H_2O$ (1) in the solid state

2.1.1. FTIR spectrum

The FTIR spectrum of **1** is depicted in the range 400–4000 cm^{-1} (Fig. S1). The strong absorption of the characteristic V=O_t (O_t = terminal O_{oxido}-atoms) stretching vibration can be seen at 938 cm^{-1}. Furthermore, bands at ca. 802 and 717 cm^{-1} are assigned to the antisymmetric modes of vibration of the V–O–V bridges, while the symmetric modes correspond to the bands between 582 and 509 cm^{-1} [92,95]. The antisymmetric stretching vibration of phosphate may be assigned to the band at 1065 cm^{-1} and the antisymmetric bending mode at 582 cm^{-1} [86,92].

TGA.

Based on thermogravimetric and elemental analysis, the suggested formulation for the obtained NH_4^+ salt of PV14 is $(NH_4)_6[H_3PV_{14}O_{42}]\bullet 19H_2O$ (**5**) with molar mass 1870 g mol^{-1}. This compound was synthesized by modification of published procedures (see experimental section) [92,96,97].

2.1.2. Powder X-ray diffraction

Powder X-ray diffraction (PXRD) analysis was carried out on $(C_7H_{10}N)_6[H_3PV_{14}O_{42}]\bullet 7H_2O$ (**1**) to verify the identity and phase purity of the crystalline material. Fig. S2 shows the measured and calculated powder diffraction pattern (based on the monocrystalline structure), which defines and confirms the phase purity of the sample.

2.1.3. Single crystal X-ray diffraction analysis

Compound **1** crystallizes in the monoclinic $P2_1/n$ space group, and its asymmetric unit contains one three-fold protonated phosphotetradecavanadate $[H_3PV_{14}O_{42}]^{6-}$ anion and six crystallographically independent centrosymmetric benzylammonium cations. Seven hydration water molecules, disordered over 7 positions, complete the asymmetric unit of 1, Fig. 1.

The $[H_3PV_{14}O_{42}]^{6-}$ anion is structurally related to the archetypical Keggin-type cluster, exhibiting two capping vanadate units at opposite regions of the framework. This arrangement includes a central tetrahedral $P^VO_4^{3-}$ anion, which links three $\{V_3O_{13}\}$ trimers formed by three edge-sharing VO_6 units through sharing corners. Each V center has one terminal O_{oxido} ligand with short V–O_t distances, d(V–O_t) ≈ 1.6 Å. The two additional capping units exhibit a penta-coordinated square-pyramidal $[V^VO_5]$ coordination mode [97,98]. All the V–O bond lengths and V–O–V angles (Tables S1-S2) are in good agreement with the literature data reported for related POV structures [35,54,63,87,99–102]. The bond length and bond-angle distortion indices (ID) were estimated following the Baur method [103]. The parameters procured are in the ranges of 0.087–0.157 for ID (V-O) and 0.152–0.228 for ID (O-V-O). These binding lengths and angles lie within the normal ranges and correspond to those mentioned in the Keggin anion literature. Bond Valence Sum calculations (BVS) justify the formulation of the cluster anion of **1** as $[H_3P^VV^V_{14}O_{42}]^{6-}$ and allowed us to locate the protonation sites. BVS calculations using the Brown and Altermatt methods showed that all V atoms have valence values ranging from 4.914 to 5.125 (avg. 5.05), confirming the formal oxidation state V^V for all metal centers (Table S3) [104–106]. The bond valence sum values for the oxygen atoms in the polyanion are in the 1.590–2.081 range, except for the bridging O(14), O(30) and O(39), these showing values of 1.262, 1.456 and 1.312 respectively, which indicates that these O atoms are protonated.

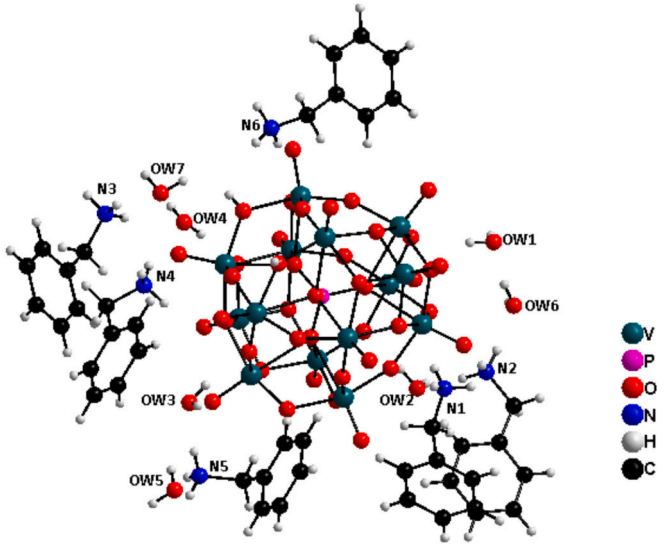

Fig. 1. Ball & stick representation of the asymmetric unit in 1.

Six benzylammonium cations surround the PV14 anion, with C—C bonds ranging from 1.347 to 1.512 Å and N-C distances around 1.486 Å. The C–C–C angles of this ion are in the range of 117.69–120.34° and around 113° for C–C–N (Tables S1-S2). Analysis of the crystal structure of **1** using a combination of Hirshfeld analysis, and manual structural analysis allowed to identify a range of highly directed intermolecular interactions which are considered to contribute significantly to the packing in the crystalline network. This structural analysis revealed that the crystal packing in the title compound is stabilized by an extensive N–H···O, O–H···O and O_w–H···O type hydrogen bonding network established between organic molecules, POV surface O-atoms and lattice water molecules. This reflects the potential of the PV14 anion to establish hydrogen bonds. Detailed hydrogen bonding parameters are given in Table S4.

Along the crystallographic [001] direction, short intramolecular N-H···O interactions established between one POV O-atom and a N-atom of the amine groups allows PV14 moieties to connect to each other in a zigzag chain. These are then further arranged into a hydrogen-bonded bidimensional network through the contact established by hydration water molecules, and protonated O-atoms from the POV surface O(14) and O(39). These layers stack along the crystallographic [100] direction involving benzylammonium cations, hydration water molecules and PV14 units to build a 3D-supramolecular architecture, as shown in Fig. 2.

2.2. Hirshfeld surface analysis

Cations and anions of **1** are connected by a three-dimensional network of N–H···O and O–H···O type hydrogen bonding interactions (Table S4) involving POV surface O-atoms and amino groups from the organic moieties. To gain more insight into the intermolecular interactions, a Hirshfeld surface analysis was carried out using Crystal Explorer 3.0 [107] and constructed by applying Eq. (1) [108]:

$$dnorm = \frac{di - rivdw}{rivdW} + \frac{de - revdW}{revdW} \quad (1)$$

where *de* is the distance from such a point to the next neighbor outside the surface, *di* is the distance to the nearest nucleus internal to the surface and *rivdW* and *revdW* are the van der Waals radius of the atoms, internal and external, respectively.

If an interatomic distance is shorter than the sum of the van der Waals radii, a red area is found on the Hirshfeld surface. All other colored regions indicate interatomic distances longer than the sum of the van der Waals radii (Fig. S3). Further interpretation of the 3D Hirshfeld surface is not straightforward and, therefore, a fingerprint plot can be constructed representing a 2D view of the 3D surface. The weaker and longer contacts other than hydrogen bonds are present in the *dnorm*

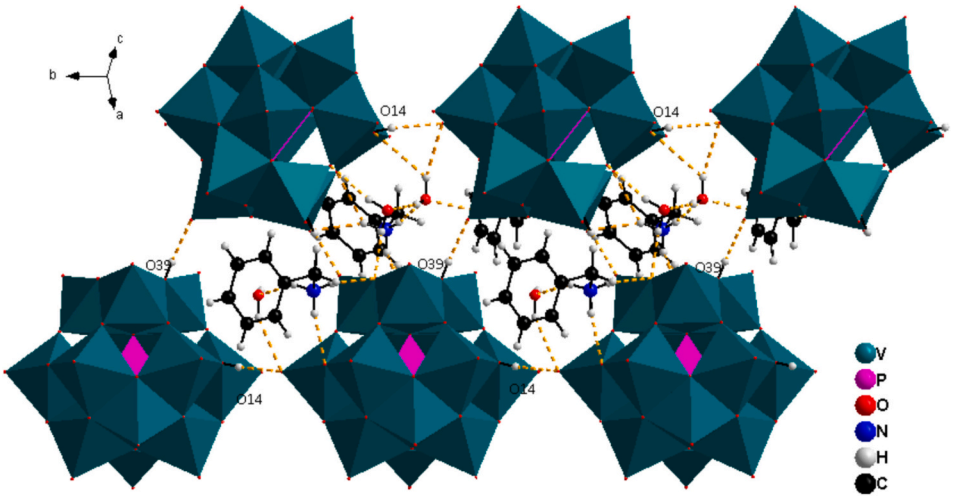

Fig. 2. Arrangement of PV14 units within the (111) plane in 1. Hydrogen bonding interactions are depicted as dashed lines.

surfaces by the other smaller extents of visible red spots and light-white regions. Hydrogen bond interactions are also evident in the shape-index (Fig. S4) by a blue convex region around the donor atom and a complementary red concave region around the hydrogen bond acceptor.

The quantitative analysis (2D fingerprint plots) was deconstructed to highlight particular atom-pair close contacts are depicted in Fig. S4. The relative contributions of individual intermolecular interactions at the Hirshfeld surface mapped over the ranges −0.728 (red) to 1.645 (blue)

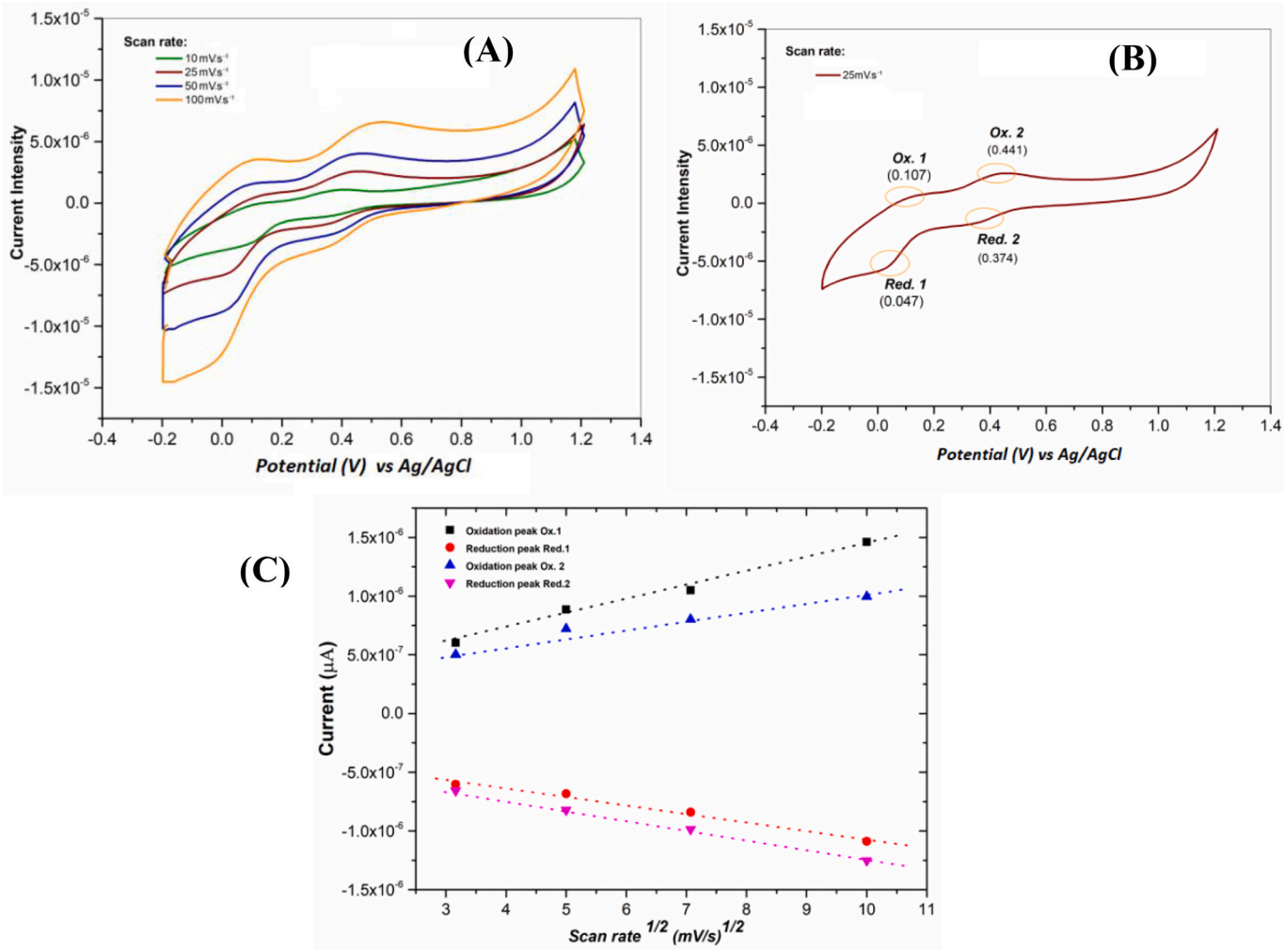

Fig. 3. Electrochemical measurements on solutions of compound 1 (1.0 mM) in 0.1 M H_2SO_4 solution. (A) Cyclic voltammograms of PV14 with various scan rates, (B) cyclic voltammogram with a scan rate of 25 mV/s, (c) peak current density vs. square-root of scan rate for peaks *Ox 0.1 / Red. 1* and *Ox 0.2 / Red. 2.* (For interpretation of the references to colour in this figure legend, the reader is referred to the web version of this article.)

are displayed in Fig. S3.

In the crystal packing, the O···H/H···O intermolecular interactions have a more significant contribution, which comprise 45.1 % of the total Hirshfeld surface area. The H···C/C···H interactions contribute 13.0 % of the total Hirshfeld surfaces. Furthermore, the H···H interactions are displayed in the distribution of scattered points in the fingerprint plots comprising 37.9 % of the total Hirshfeld surfaces Fig. S4.

2.3. Behavior in solution

2.3.1. Cyclic voltammetry

The redox properties of 1 were investigated by cyclic voltammetry (CV) studies. Fig. 3A shows the results from the experiments with 0.1 M H_2SO_4 aqueous solutions of **1** at different scan rates (10, 25, 50, and 100 mV/s). In aqueous solution PV14 anions may have significant concentrations in the pH range 1.5–4.0, and for adequate concentrations of the total vanadium ($[V]_{total}$) and total phosphate ($[P]_{total}$). For pH < 1.5 the VO_2^+ species predominates, and in the pH range 2–6 decavanadate anions may predominate or form in significant proportion. Speciation calculations for a PV14 concentration ([PV14]) of 1 mM (corresponding to $[V]_{total}$ = 14 mM and $[P]_{total}$ = 1 mM), using the formation constants of Selling et al. [109] (see Fig. 4), predict that at the pH of the CV measurements the risk of decomposition of PV14 is relevant. So, although upon dissolution the PV14 anion of **1** may persist for several hours [22,109], the redox properties of the PV14 anion, as well as of other ions resulting from its decomposition, may be contributing to the cyclic voltammograms recorded. Our CV results are quite similar to those reported by Friedl et al. [22] mostly carried out in solutions with 1 M H_2SO_4, where the authors assumed that the PV14 anions preserved its integrity during the redox processes.

As highlighted by Friedl et al. [22] and Huang et al. [110], the redox waves associated to PV14 involve multi-electron processes; for example, during the oxidation at least 5 electrons are transferred. Therefore, the overlap of several redox reactions does not allow the determination of the exact standard potentials and peak separations. In the potential range − 0.4 to +1.4 V, at least two oxidation and two reduction waves are observed corresponding to *Ox. 1 / Red. 1* and *Ox. 2 / Red. 2* (Fig. 3B). The measured mean peak potentials $E_{1/2} = (E_{pa} + E_{pc})/2$ are 0.077 V (1) and 0.407 V (2) (scan rate: 25 mV/s) with E_{pa} and E_{pc} being the anodic (oxidation) and cathodic (reduction) peak potentials, respectively. Fig. 3C shows that the peak currents of the redox process are proportional to the scan rate, and the linear dependence of peak current vs. the square root of the scan rate reveals that these are diffusion-controlled processes.

Quantum mechanical density functional theory computational studies presented below confirm the inherent tendency of PV14 anions to accept electrons at sufficiently low pH as well as the possibility of forming stable mixed-valence reduced forms, which justifies the appearance of multi-electron redox waves at negative electrode potentials.

At this point we highlight that a PV14 concentration ([PV14]) of 1 mM corresponds to a total vanadium concentration ($[V]_{total}$) of 14 mM and to a total phosphate concentration ($[phosphate]_{total}$) of 1 mM. The species distribution diagram predicted for PV14 concentration ([PV14]) of 1 mM (Fig. 4) indicates that, in equilibrium conditions, the PV14 anions comprising three protonation states, H_3PV14^{6-}, H_4PV14^{5-} and H_5PV14^{4-}, are not the major species in solution. Notwithstanding, it has been reported that, in the pH range 2–3.5, the PV14 anions are kinetically inert and decompose slowly [22,109]. Therefore, at this concentration and pH the risk of decomposition of PV14 is moderate, the redox properties of the PV14 anion being likely observed. Note that, among the PV14 species present, at the pH of the CV experiments H_5PV14^{4-} and H_4PV14^{5-} are the most relevant ones.

2.3.2. ^{51}V NMR spectra of solutions of PV14 anions

Fig. 5 depicts the ^{51}V NMR spectra of a 2 mM aqueous solution of the prepared NH_4^+ salt of PV14, formulated as $((NH_4)_6[H_3PV_{14}O_{42}]\bullet 19H_2O$ (**5**) at pH 2.5. The corresponding ^{31}P NMR spectra are depicted in Fig. S5. Note that with $[PV14]_{total}$ = 2 mM, the $[V]_{total}$ is 28 mM, thus the solution is quite concentrated in terms of total V^V present. The peak at −544 ppm is due to monovanadates (V1) and its relative amount increases with time.

According to Selling et al. [109], the bands at −532/−533, −586/−587 and − 598 ppm correspond to the ^{51}V NMR chemical shifts (δ_V) of V^V atoms of PV14 anions That were designated as V(3), V(2) and V(1). Because of the possible presence of other V-containing species we are using here the designations PV14–3, PV14–2 and PV14–1, respectively. The PV14 anions have a *trans*-bicapped α-Keggin structure, corresponding to 3 types of non-equivalent V-atoms. One type includes the

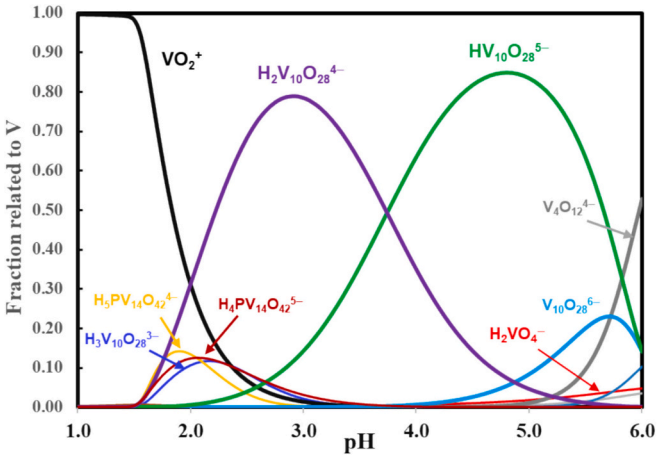

Fig. 4. Species distribution diagram representing the total fraction of V corresponding to each vanadium-containing species, as predicted for solutions containing [PV14] = 1.0 mM in the pH range 1–6. This corresponds to $[V^V]_{total}$ = 14.0 mM and $[phosphate]_{total}$ = 1.0 mM. The diagrams were calculated using the HySS computer program [111] including the hydrolytic species (see Materials and Methods section) and using the formation constants of refs. [86], [109] and [112].

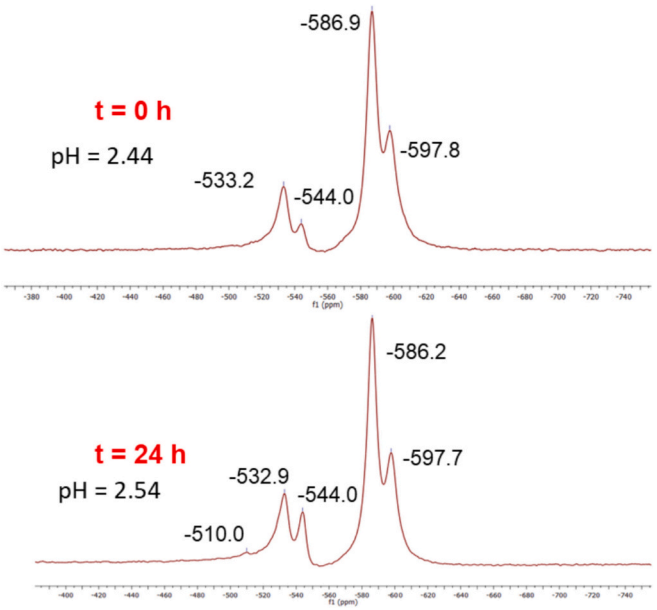

Fig. 5. ^{51}V NMR spectra of a 2 mM solution of 5 immediately after preparation and after 24 h. HCl was added to the solution so that the initial pH would be close to 2.5. The ^{51}V NMR spectra of compound **1** in similar conditions (pH, concentration and time after preparation) are identical.

two capping V-atoms that are 5-coordinated to O-atoms, which give rise to the ^{51}V NMR peaks PV14–3. All the remaining 12 vanadiums are 6-coordinated. Eight of these are connected to the capping V-atoms (four to each) which structurally differ from the remaining four (peaks PV14–2 and PV-14-1, respectively). On the other hand, the PV14 anions may have different protonation states and at pH ~2.5 the main ones are H_4PV14^{5-} and H_5PV14^{4-}.

The V10 anions, if present, may remain structurally intact in solution and contain three different types of vanadium atoms according to their position in the polyanion structure. These are often labelled as V10A, V10B and V10C. In this work we labelled as V10C the six-coordinate non-oxido V-atoms that are buried within the V10 polyanion; these are the V atoms less sensitive to changes in the solution media, such as modifications of pH. The outer vanadium atoms containing a V=O group are labelled V10B and V10A; these atoms are surface accessible and show the greatest sensitivity to the pH of the solution. From the thermodynamic point of view, decavanadates should correspond to ~50 %, and the PV14 anions to ~40 % of total V^V in these conditions (see Fig. S6). Observing the recorded ^{51}V NMR spectra at $t = 0$, no peak due to V10 is clearly visible, but at $t = 24$ h the small band at around −510 ppm could originate from the V^V atoms designated by V10B. The peak of V^V atoms designated by V10C should appear at ~ −425 ppm, but are not detected, and that of V10A at ~ −526 ppm. Thus, PV14 anions show appreciable kinetic stability as evidenced by peaks due almost only to V^V atoms of PV14 are observed. We remark that the ^{51}V NMR spectra of a solution containing 2 mM of compound **5** and 8.0 mM of benzylamine immediately after preparation and after 24 h (Fig. S7) do not present any significant difference from those of Fig. 5. Interestingly, at lower concentration of the PV14 compounds (0.90 mM, see Fig. S8 for **1**) the ^{51}V NMR spectra are similar but the three peaks due to decavanadate are now clearly visible at −425 (V10C), −507 (V10B) and ~ −527 ppm (V10A), this demonstrating the relevance of $[V]_{total}$ values in the speciation of vanadium containing species in solution.

These particular spectra are also quite similar to those of $(C_6H_{14}N_4)_2(NH_4)[H_4PV_{14}O_{42}]\cdot 11H_2O$ [86], at pH = 2.3 (in water), where $C_6H_{12}N_4$ is methenamine. In contrast with these results obtained at low pH values, in aqueous solution at pH ~7, as evaluated by both ^{51}V NMR and UV–Vis spectroscopy, the PV14 anions were not stable, and the hydrolysis proceed faster as the $[V]_{total}$ decreased. This phenomenon is considered in ref. [87] and extensively discussed in ref. [37]. It is also addressed in the Supplementary Materials section. Moreover, PV14 polyanions are not stable at pH = 7. So, once dissolved in a media of this pH they tend to hydrolyse. Upon the dissolution of the PV14 **1** at 2 mM concentration, this polyanion hydrolyses and the main V-species detected by ^{51}V NMR after ~0.1 and 3 h of preparation are V1 (monovanadates), V2 (divanadates), V4 (tetravanadates), as well as small amounts of decavanadate.

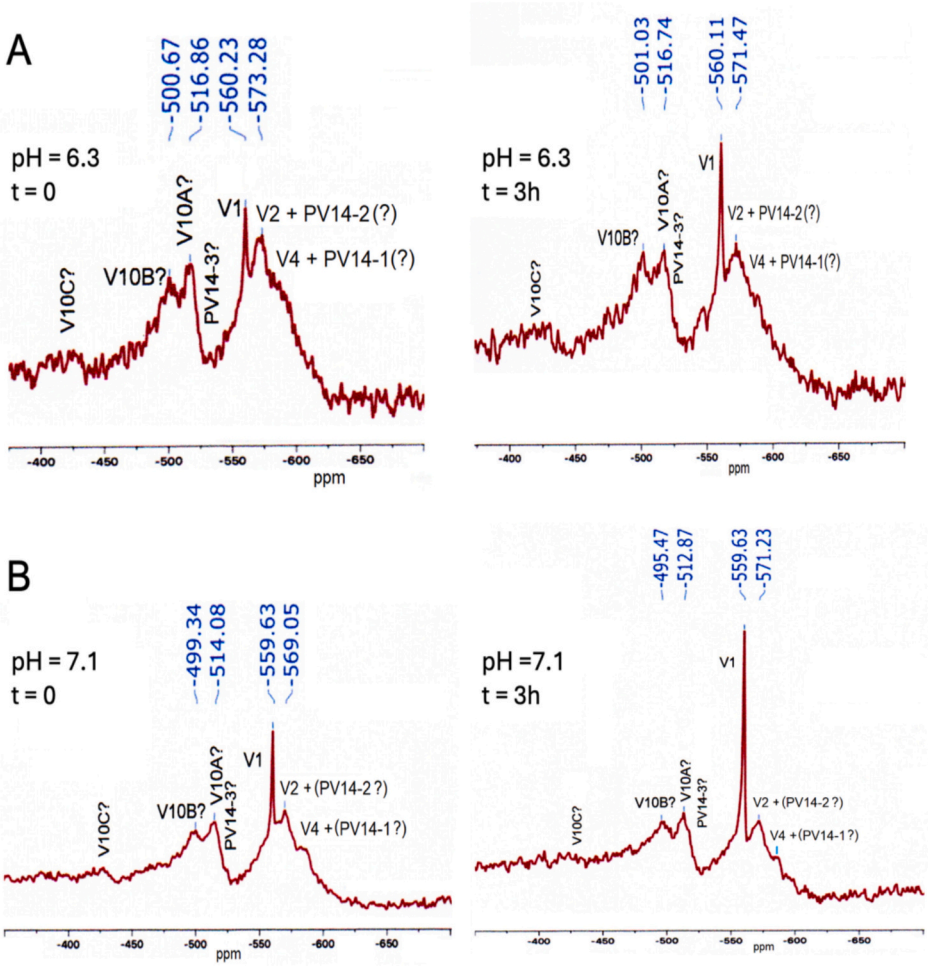

Fig. 6. ^{51}V NMR spectra of a 0.90 mM solution of **1** and HSA (0.60 mM) immediately after preparation and after 3 h (A) at pH = 6.3; (B) the same at pH = 7.1. The solutions were prepared by adding compound **1** to solutions of HSA in Hepes buffer (5.0 mM) with the pH adjusted to either 6.3 or 7.1. Several V^V species may show up at very close regions of the ^{51}V NMR spectra, and their bands becoming broader due to interactions with HSA; so, there may be extensive superposition of the corresponding ^{51}V NMR bands. Therefore, as we are not sure of their presence, we include '?' in the identification of some of these V^V species in the figure.

2.3.3. ^{51}V NMR spectra of solutions containing PV14 compounds and albumin

In one of our previous works [87], we showed that the PV14 anions interact with bovine serum albumin (BSA), the albumin present in mammalian cell incubation media. Encouraged by those results, in this work we carried out several experiments with solutions containing human serum albumin (HSA) and compounds **1** and **5**. HSA is the albumin present in human serum and the protein responsible for transport of many nutrients and therapeutic drugs. HSA and BSA have many similarities but it may happen that their binding to V10 or PV14 anions may differ. In this work one of our aims was to demonstrate the binding of PV14 polyanions to HSA.

Fig. 6 depicts ^{51}V NMR spectra of a 0.90 mM solution of **1** and HSA (0.60 mM) immediately after preparation and after 3 h. According to Selling et al. [109] at pH ~6.3 the peaks of V^V atoms PV14–3, PV14–2 and PV14–1 correspond to δ_V values of −515, −566 and − 583 ppm, respectively, and peaks close to these values are indeed observed. According to Pettersson et al. [110], at pH ~6.3 the δ_V values of V^V atoms of decavanadates correspond to approximately −514 (V10A), −495 (V10B) and − 424 ppm (V10C), and V1 at −559 ppm. All these are visible in the spectra of Fig. 6, almost all of them corresponding to rather broad bands. This broadening of ^{51}V NMR peaks indicates the establishment of interactions of the corresponding PV14-species with albumin. At pH ≥ 6.3 no significant amounts of PV14 or V10 anions are expected to exist in solution (Fig. 7) [112], so, the observation of bands due to these species are an additional indication of the binding of PV14 (and V10) anions to HSA. At $t = 3$ h the sharp peak due to V1 emerges with increased intensity when compared with the spectrum recorded at $t = 0$. This also suggests that V1 binds rather weakly to HSA. Additionally, the shoulder band between ca. -570 and − 620 ppm, with contributions of V^V atoms of V2 and PV14–2 and of V4 and PV14–1, respectively, slightly broadens, probably due to an increase in the relative amount of V2 and V4. In the ^{51}V NMR spectra similarly recorded but at pH ~7.1 (Fig. 7B), the amounts of V1, V2 and V4 are higher than those observed at pH 6.3.

2.4. Computational study

This section presents a computational study based on quantum mechanical density functional theory (DFT) and molecular dynamics (MD) simulations, to gain a deeper insight into some physicochemical characteristics of the PV14 system. We present complementary information related to the $[PV_{14}O_{42}]^{9-}$ anion and some of its protonated forms, as well as the dynamic behavior obtained in a model environment that mimics the solution conditions. We discuss the internal structure, the relative stability of several protonated forms and the molecular orbital sequence in aqueous solution. Also, we show how PV14 is surrounded by the solvent and the electrolyte ions in an aqueous solution, as is the case in the present work. We emphasize that the protonation ability of a POM, besides determining its overall charge, is important for the establishment of strong interactions with e.g. biologically relevant molecules or cell membranes. On the other hand, the ability of POVs to be involved in redox processes may be important for their biological activity [37].

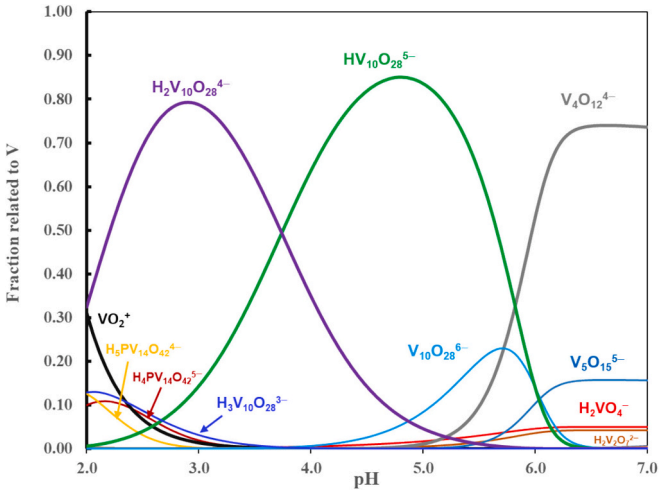

Fig. 7. Species distribution diagram representing the total fraction of V corresponding to each vanadium-containing species, as predicted for solutions containing [PV14] = 0.90 mM in the pH range 2–7.5. This corresponds to $[V^V]_{total}$ = 12.6 mM and $[phosphate]_{total}$ = 0.90 mM. The diagrams were calculated using the HySS computer program [111] including the hydrolytic species (see Materials and Methods section) and using the formation constants of refs. [86], [109] and [112].

Structural parameters obtained by full geometry optimization of $[PV_{14}O_{42}]^{9-}$ and its tetra-protonated form as $[(H_3O)_4PV_{14}O_{42}]^{5-}$ at the DFT level (Table 1, indicated as H_4PV_{14}) show very good agreement with experimental data, the penta-protonated form showing similar good agreement (see ESI, Tables S5-S9 for nuclear coordinates of the calculated structures). As expected, protonation does not have a deep impact on the selected distances irrespective of the number of protons added to the structure. Interatomic distances for $[(H_3O)_xPV_{14}O_{42}]^{(9-x)-}$ (x = 1–3 and 5) anions can be found in Table S10. Considering the general good match between theoretical and experimental data, the electronic analysis of these structures will shed some light on fundamental properties of the anions.

The frontier molecular orbitals of the fully oxidized, non-protonated $[PV_{14}O_{42}]^{9-}$ system with formally all V^V-centers, present similar features to other POV systems (Fig. 8A). The highest occupied molecular orbital (HOMO) has an energy of −6.692 eV, and − 3.051 eV is the value found for the lowest unoccupied molecular orbital (LUMO). Compared to our previous work [86,87] these energies are more negative due to the use of a hybrid functional in the present study, concomitant with a larger HOMO-LUMO energy gap (Fig. 8C). Regardless of the theoretical level used, however, the HOMO is a combination of p-type oxygen orbitals and the LUMO has mostly nonbonding character of d-type vanadium orbitals. The high symmetry and delocalized nature of the LUMO (Fig. 8A) reinforces the chemical quasi-equivalency of all V centers, implying that that reduction of the system would generate delocalized extra electrons.

Considering the nature of the aqueous solution and the experimental evidence of protonation, several protonated and reduced species of $[H_xPV_{14}O_{42}]^{(9-x)-}$ were analyzed. A reliable property to identify the geometrical positions of protonation sites is the molecular electrostatic potential and the derived *potential wells*, interpreted as the most nucleophilic regions of the molecule. Fig. 8B represents the four wells (green surfaces), equivalent due to the molecular symmetry, with the most negative potential in the fully deprotonated species. In vanadium- or tungsten-based POMs, M-O-M bridging oxygen sites tend to be protonated first [113,114]. In the present structure, these positions are located in the $[M_4O_4]$ structural motifs, which are surrounding each potential well in the figure. These are the four principal protonation sites for $[PV_{14}O_{42}]^{9-}$. The homologous potential wells for the species

Table 1
Interatomic distances (Å) for the DFT-optimized structures of $[PV_{14}O_{42}]^{9-}$ and $[H_4PV_{14}O_{42}]^{5-}$.

	PV_{14}	H_4PV_{14}
$P–O_{tetr}$	1.545	1.544–1.553
$V–O_{tetr}$	2.375–2.396	2.390–2.434
$V_{cap}–O_{tetr}$	3.227	3.240–3.281
$V–O_{term}$	1.631–1.636	1.605–1.615
$V_{cap}–O_{term}$	1.643	1.621
$V–O_{brige}$	1.759–2.082	1.777–2.046
$V_{cap}–O_{bridge}$	1.827–1.916	1.838–1.933
$V–V_{cap}$	3.034	2.962–3.086

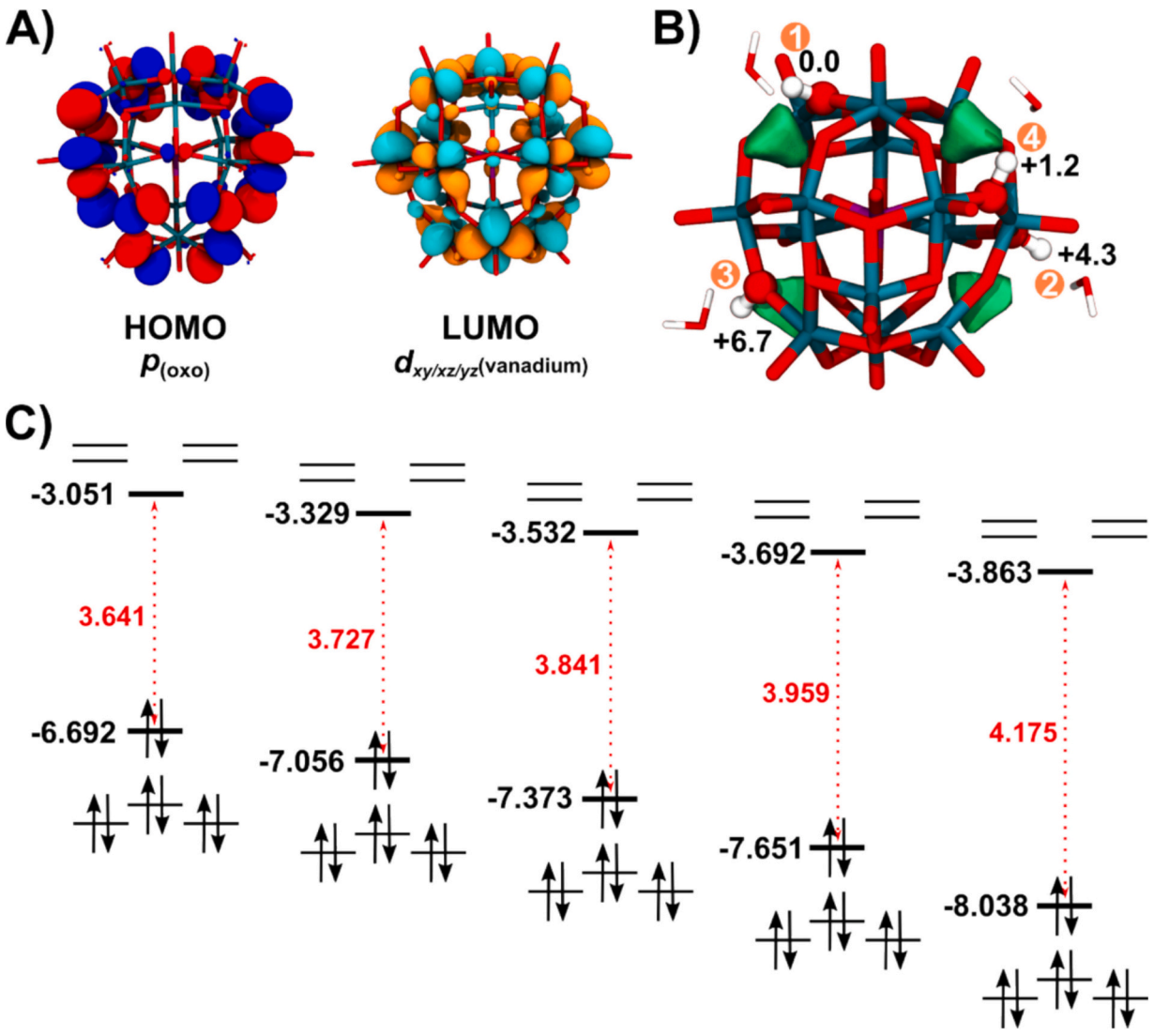

Fig. 8. Electronic characteristics of the $[H_xPV_{14}O_{42}]^{(9-x)-}$ anions. (A) Representation of the HOMO and the LUMO of the non-protonated form ($x = 0$). (B) Electrostatic potential wells of $[PV_{14}O_{42}]^{9-}$ as green surfaces, and successive protonation energies in kcal mol^{-1}, relative to the first protonation indicated as 1. (C) Frontier molecular orbital energies and HOMO-LUMO gaps, in eV, for the $[H_xPV_{14}O_{42}]^{(9-x)-}$ series ($x = 0$–4, from left to right). (For interpretation of the references to colour in this figure legend, the reader is referred to the web version of this article.)

$[(H_3O)_xPV_{14}O_{42}]^{(9-x)-}$ ($x = 1$–4) are shown in Fig. S9. After obtaining the $[(H_3O)_xPV_{14}O_{42}]^{(9-x)-}$ ($x = 0$–5) optimized geometries and their relative energies, protonation energies (PEs) were calculated as:

$$[(H_3O)_xPV_{14}O_{42}]^{(9-x)-} + H_3O^+ \rightarrow [(H_3O)_{x+1}PV_{14}O_{42}]^{(8-x)-}.$$

using −18.711 eV as the energy for the hydronium release from a water cluster for being incorporated to the POV structure, as shown in the Computational Details section [87]. A deeper analysis was performed to know which O atom of the $[V_4O_4]$ motif is preferentially protonated. Fig. S10 in the SM section reveals a tiny energy difference of 0.3 kcal mol^{-1} between the two cases. This value can be interpreted as both oxygen sites having effectively the same tendency to bind a proton. In our calculations, the presence of one explicit water molecule close to the proton in the protonated derivatives confers the system with a highly realistic geometry and energy.

Computed successive protonation energies (PE, in kcal mol^{-1}) for the $[PV_{14}O_{42}]^{9-}$ system (abbreviated as $H_xPV_{14}^{n-}$).

The PEs shown in Table 2 are mostly exothermic, indicating that the $[PV_{14}O_{42}]^{9-}$ anion can be protonated several times in certain (acidic) conditions, at least from thermochemical arguments. The first two processes are highly stabilizing and, given that the PE difference between the third and the fourth protonation is 1.2 kcal mol^{-1} only, we suggest that the $[H_3PV_{14}O_{42}]^{6-}$ and $[H_4PV_{14}O_{42}]^{5-}$ species could coexist as major species in similar amounts. This is in line with the observations of Selling et al. [109] about the speciation of tetradecavanadate anions in water. The penta-protonated species, if maintaining the fully oxidized form, has a lower tendency to dominate, although at very low pH it must be considered since it is degenerate in energy with the tetra-protonated one. These values change dramatically when higher reduction states are considered for the PV14 species. For example, the protonation of the 2e-reduced form H_2PV_{14} $2e^{9-}$ involves a reaction energy of −17.30 kcal mol^{-1}, considerably more exothermic than the

Table 2
Computed successive protonation energies (PE, in kcal mol^{-1}) for the $[PV_{14}O_{42}]^{9-}$ system (abbreviated as $H_xPV_{14}^{n-}$).

Protonation reaction	Absolute PE	PE relative to the previous protonation
$PV_{14}^{9-} \rightarrow HPV_{14}^{8-}$	−21.32	0.0
$HPV_{14}^{8-} \rightarrow H_2PV_{14}^{7-}$	−17.05	+4.3
$H_2PV_{14}^{7-} \rightarrow H_3PV_{14}^{6-}$	−10.37	+6.7
$H_3PV_{14}^{6-} \rightarrow H_4PV_{14}^{5-}$	−9.19	+1.2
$H_4PV_{14}^{5-} \rightarrow H_5PV_{14}^{4-}$	0.00	+9.2

non-reduced partner species.

Fig. 8C shows schematically how the frontier molecular orbital energies decrease as protons are added to the compound, from left to right, a typical consequence of decreasing some anion charge by protonation. Alongside, we observe that the HOMO-LUMO gap becomes larger, altogether conferring progressively more stability to the system. We observe an interesting feature related to the four-fold protonated form, arising in two ways. First, going from H_3PV_{14} to H_4PV_{14} produces the largest HOMO-LUMO gap increase (0.216 eV) between two successive members of the series, whereas the previous three protonations generate variations in the range 0.086–0.118 eV. Second, the fourth PE is more exothermic than expected from a global view of the series (Table 2). So, if the relative PE change is sustained, a PE close to zero, or even positive, would not be surprising. A possible explanation for these features is that, after the fourth protonation, the POM system recovers some symmetrical arrangement, with the four $[V_4O_4]$ motifs protonated. This fact makes the H_4PV_{14} form different from the other three protonated anions. The fifth protonation of the fully oxidized system (all V^V) gives a formally non-favorable process, although in reduced form this becomes a favorable one.

Expectedly, when the POV is populated by extra electrons, the molecular orbitals are shifted to higher (less negative) energies, a trend that helps tracking the loss of stability of the system. A rather general fact is that, if two or more different species with the same framework carry the same negative charge (i.e., $[H_4PV14 + 4e]^{9-}$ and $[H_2PV14 + 2e]^{9-}$ and $PV14^{9-}$), the molecular orbital energies are found at similar energies. In this case, the highest oxido orbitals are found at −6.58, −6.65 and −6.69 eV. In contrast, by keeping the number of protons but changing the number of electrons (i.e., $[H_4PV14 + 4e]^{9-}$ and $[H_2PV14 + 4e]^{11-}$) gives −6.58 and − 5.96 eV, deducing that the former species will predominate at acidic pH. These values explain the importance of the molecular charge in understanding speciation in POMs.

A more complete view of the reduction-protonation phenomena can be found in Table S11, in which diverse pure reduction and protonation processes, as well as proton-coupled electron transfer (PCET) processes, are listed. The reader may notice that reduction and PCET processes involve two electrons each. Since this inspection is mostly trend-oriented, this aspect is not relevant. So, the information is highly significant because it denotes the stability and probable abundance of the different species as the number of protons and electrons populate the PV14 structure. One outstanding fact is that all processes are exothermic, notably the PCET ones presented as, for example, $POM + 2H^+ + 2e \rightarrow [H_2POM + 2e]$. When the overall charge of the POM remains constant by a PCET because the electrode potentials are adequate, reduction and protonation can occur simultaneously. Within PCET processes, those having the oxidized form of the POM as reactant are the most favored ones (total reaction energies close to −200 kcal mol^{-1}), denoting that non-reduced forms of the POM are not expected in acidic conditions. From the same table, it can be easily inferred that pure reduction processes are more favorable (more negative reaction energies) when the protonation degree is high (and the POV charge is lower) and, conversely, pure protonation processes are more favored for highly reduced systems. Thus, these results confirm the formation of highly reduced forms (i.e., appearance of multi-electron redox waves at negative electrode potentials) if the pH is sufficiently acidic, given the inherent tendency of the PV14 moiety to accept electrons. These features are probably relevant for the biological effects demonstrated by PV14 species.

MD simulations provide additional information on the dynamic behavior of 1 in solution. The results are treated as an average for the simulated time and a box containing five H_4PV_{14} units (as representative species at low pH) with the corresponding benzylammonium cations to fulfill electroneutrality, and water as solvent for the solute (**1**) concentration of 28 mM. The analysis is summarized in Fig. 9, revealing the expected absence of aggregation between POVs in aqueous medium, manifested as the lack of a peak at short distances (first sign of $H_4POV\cdots H_4POV$ interaction at 15 Å). This fact is ascribed to the high hydrophilicity of H_4PV14, giving an average stabilizing interaction with water molecules of ca. -790 kcal mol^{-1} per POV unit. Solvation of H_4PV14 units is compelled by hydrogen bonds through acceptor O-atoms of H_4PV14 by ca. 150 water molecules per cluster. Some aggregation between benzylammonium cations and POV moieties was detected, but they are not long-lived (around 1 cation on average for 10 ns of simulation). Two hydrogen bond-controlled coordination modes can be identified: direct N-H···O-V and N-H···O_w-H···O-V. This behavior is commonly found in similar metal-oxido clusters in water [115].

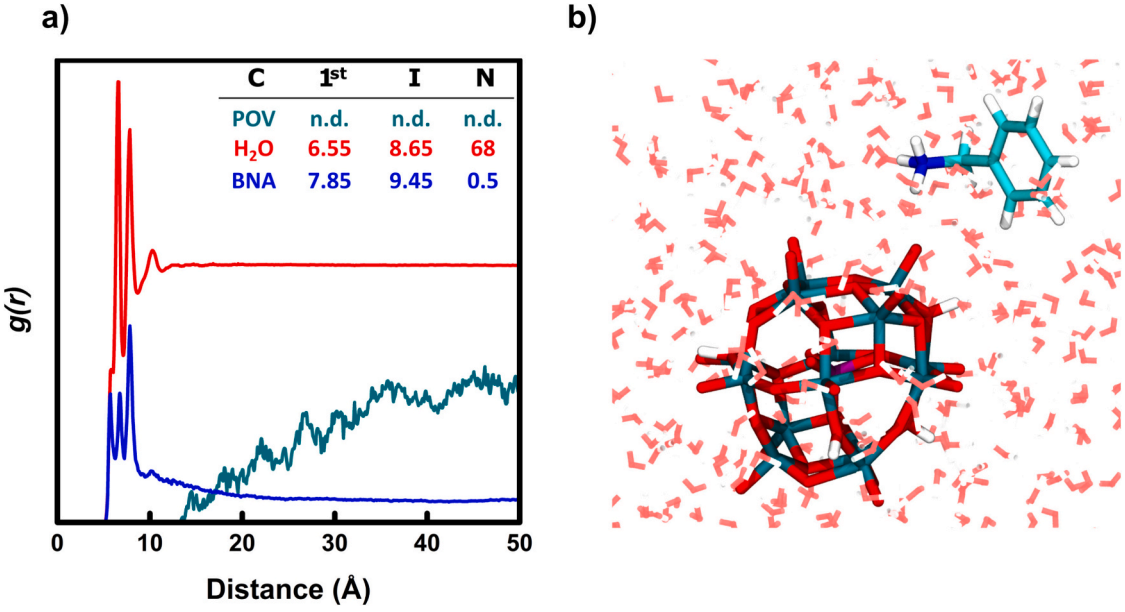

Fig. 9. (a) Superposition of Radial Distribution Functions, $g(r)$, for the fully oxidized $H_4PV_{14}\cdots H_4PV_{14}$ (turquoise), H_4PV_{14}··benzylammonium (BNA) (blue) and $H_4PV_{14}\cdots H_2O$ (red). The first peak(s) (1st), the integration distance (I), both in Å, and the average coordination number (N) are given. The vertical scale is different and arbitrary for each curve. (b) Snapshot representing one interaction motif between H_4PV_{14} and benzylammonium (water molecules depicted as translucent red/white cylinders). (For interpretation of the references to colour in this figure legend, the reader is referred to the web version of this article.)

Nevertheless, the POV···water interaction dominates the POV environment (−37.7 kcal mol^{-1} per POV unit between POV···benzylammonium). In conclusion, we suggest that the effect of the counter ions on the POV activity is negligible in the working conditions.

2.5. Effect of compound 1 on U87 glioblastoma cell viability

Compound **1** was tested at different concentrations (from 200 μM to 0.1 μM) on the viability of U87 glioblastoma cells by the MTT assay (see experimental section). We found that the compound inhibited the viability of U87 cells with a half maximal inhibitory concentration (IC_{50}) of 3.2 ± 0.6 μM and 1.10 ± 0.04 μM after 24 h and 72 h treatment, respectively (Fig. 10). These results showed that compound **1** acts as anti-proliferative agent.

We must emphasize that cell media contain many potential ligands for V^V, and its speciation may be very complex, and the cytotoxic effects observed may be due to several distinct VCs formed in the cell medium over time [37,84,116–119]. In fact, the IC_{50} values of 3.24 μM and 1.10 μM correspond to $[V]_{total}$ of 45.4 and 15.4 μM, respectively. In aqueous solution of pH = 7 containing a V^V salt with these concentrations, speciation calculations predict that the main V^V-species present are $H_2VO_4^-$ and HVO_4^{2-}. To our knowledge the cytotoxicity of vanadate(V) salts was never tested on U87 cells, but for most cancer cells tested the IC_{50} values are >50 μM [62,120], and for T98g glioblastoma cells an IC_{50} (at 24 h) of 26 ± 4 was reported [116]. Consequently, we anticipate that the observed U87 cell death may have contribution from monovanadates (V1). We also note that, besides PV14, in cell media several vanadium-containing species may be present, namely V10, V1 and V2, and these species may bind to ligands present in the medium, for example: BSA, glucose, amino acids and phosphates [37,62], the formation of complexes favoring some V-species as compared to others. However, there is no available literature data to allow us to predict which species might predominate. Upon uptake by cells, there are further aspects that make the identification of the active species, namely possible reduction of the V^V-containing species. Ascorbate, cysteine and glutathione are some of the major reducing agents found in biological systems, and all may reduce the V^V –species uptaken. [36,37,39,121–124]

The data obtained in this study showed that, in molar units, compound **1** is at least 38 times more active than TMZ, the current first-line drug used against glioblastoma [72–75]. Indeed, TMZ showed mean IC_{50} values of 123.9 and 230 μM on the viability of U87 cells after treatments for 24 and 72 h, respectively [74]. On the other hand, several vanadium-based molecules, including POV compounds, showed anti-cancer activity on glioblastoma cells [63,78,81,90,91]. In molar terms most of these compounds had less important effects than the phosphotetradecavanadate compound described in this work; nevertheless, we highlight again that PV14 concentrations of 3.24 μM and 1.10 μM correspond to $[V]_{total}$ of 45.4 and 15.4 μM. Therefore, these data suggest that PV14 compounds deserve further studies to evaluate their potential therapeutic value against glioblastoma.

The viability of U87 glioblastoma cells after treatment for 24 and 72 h was also evaluated with compound **5**, an ammonium salt of PV14, as well as with benzylamine (Fig. S11). Since the cytotoxic effects observed with **5** are quite close to those of **1**, and that the organic cation alone has no significant effect on these cells, we may conclude that the observed effects of compound **1** are due to PV14 and/or other species resulting from it in solution. In the MD simulations carried out to evaluate the dynamic behavior of compound **1** in solution, a concentration of 28 mM was used and no important binding of the benzylammonium cations to PV14 anions was detected. Furthermore, no significant differences were found, in ^{51}V NMR experiments, in the binding of **1** to HSA in the presence or absence of benzylamine in solution. Therefore, although we cannot firmly state that benzylammonium cations are not involved in the biological effects observed, our data globally indicate that there is no contribution from their presence to the cytotoxicity measured for compound **1**.

2.5.1. Pro-Apoptotic effect of compound 1

To identify relevant aspects for the mechanism of action of compound **1** on U87 cells viability, we explored the pro-apoptotic process. The U87 cells were treated for 24 h with three doses of **1**, corresponding to the IC_{50} (3.25 μM), ½ IC_{50} (1.62 μM) and 2 × IC_{50} (6.5 μM) of viability. Next the luminescence was measured to access for the apoptotic effect and fluorescence for the necrotic one. As can be seen in Fig. 11, compound **1** increased significantly the luminescence in a concentration-depending manner and increased the fluorescence independently of the used concentrations.

Fig. 11 also shows clearly the higher increase of the fluorescence compared to the luminescence in presence of H_2O_2, used as positive control for the necrotic effect. Based on these results, we can conclude that compound **1** has a pro-apoptotic effect. Our results are in line with several other studies on vanadium-based compounds reporting that these molecules trigger or increase apoptosis on different cancer cell lines [85,116,125–127].

2.6. Vanadium species responsible for the biological effects observed

As recently reported by Xu, et al., that $V^{IV}O(acac)_2$ efficiently and selectively suppress growth of U251 and GL261 glioblastoma cell lines, with IC_{50} values in the range 4 to 6 μM [79]. It is known that, at these low concentrations, $V^{IV}O(acac)_2$ extensively hydrolyses [128–130]. To improve potency and reduce toxicity issues, the authors reported the successful use of graphene oxide quantum dots as an administration route.

In aqueous solutions at pH ~7, PV14 anions are expected to display

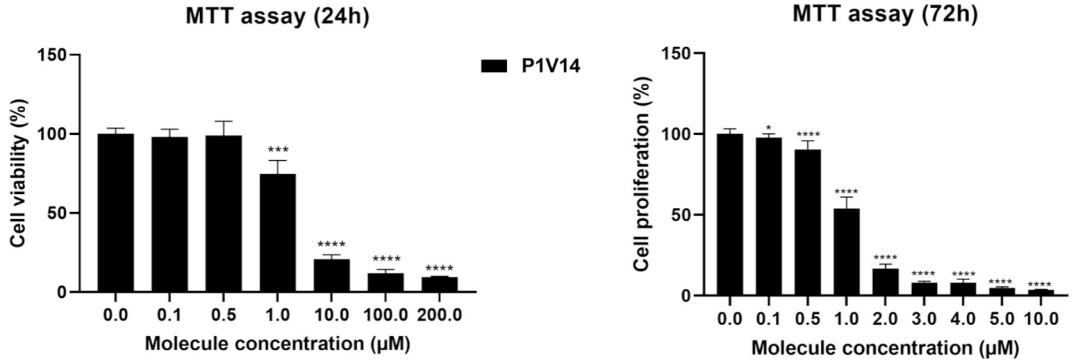

Fig. 10. U87 glioblastoma cells were treated by different concentrations of compound $(C_7H_{10}N)_6[H_3PV_{14}O_{42}]\bullet 7H_2O$ (**1**) ranging between 200 μM to 0.1 μM for 24 h, and concentrations ranging between 10 μM to 0.1 μM for 72 h, using the MTT assay. Cell viability was calculated in percent as (OD560 Sample - OD560 negative control) X 100. Each test was repeated three independent times and treated cells were compared to negative control (* $p < 0.05$, *** $p < 0.001$ and **** $p < 0.0001$).

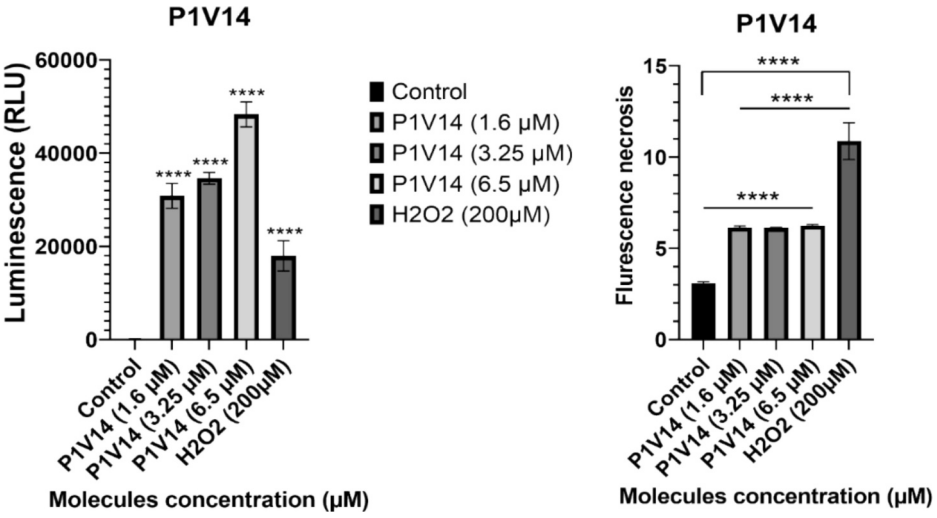

Fig. 11. U87 glioblastoma cells were treated by three doses IC_{50} (3.25 µM), ½ IC_{50} (1.62 µM) and 2 × IC_{50} (6.5 µM) of compound **1** for 24 h using the RealTimeGlo™ Annexin V Apoptosis and Necrosis Assay (OD was measured for Luminescence and fluorescence (Excitation 485 nm, Emission 525–530 nm). Each Condition was repeated three times and treated cells were compared to negative control (**** $p < 0.0001$).

extensive hydrolysis and are not predicted to exist, particularly at the low concentrations where it was found that compound **1** was effective against U87 glioblastoma cells. Remarkably, the ^{51}V NMR spectra of Fig. 6 indicates that PV14 anions may possibly exist at pH ~7 in the presence of HSA due to interactions of the PV14 anions with positive amino acid side groups of the albumin. Such type of binding was found for decavanadate anions with several proteins, and it may be tentatively extrapolated that both decavanadates and PV14 anions may also bind to BSA, the albumin present in the cell medium. However, in Fig. 6 the concentration of **1** is 0.90 mM while the IC_{50} values are in the µM range, where the propensity for the hydrolysis of PV14 anions is much higher. Notwithstanding, the molar ratio [BSA]:[PV14] is much higher in the incubation media used that in the conditions of Fig. 7, this enabling a binding to BSA and consequent stabilization of PV14 anions. Above, we highlighted the interesting finding of effects of POVs on CHO cells growth inhibition, namely of $K(NH_4)_4[H_6V_{14}O_{38}(PO_4)]$ (**3**), although it was recognized that it would only be present in the cell medium for very short periods of time. This observation led to the suggestion that the signaling with **3** was very fast [62]. Whether this may happen with compound **1** or not cannot be confirmed with the available data.

We emphasize that the correct characterization of the VC responsible for the observed biological effects either in this study or in others previously reported [37], presents additional levels of complexity. In fact, there are several reports of binding of oligomeric vanadium inorganic-based species to proteins characterized by SC-XRD or Cryogenic Electron Microscopy (cryo-EM). These include V2, V3, V4, V6, V10, V15 (V18) and V20 entities, and in some cases mixed-valence species form [54–58,131,132]. The binding normally involves non-covalent interactions, while in some cases covalent bonds are established. In many cases the starting VC is a complex of V^{IV} or V^{V} with an organic ligand that gives rise to the POV bound to the protein.

In conclusion, due to the complexity of the speciation that may be established upon interaction of the diverse molecules present in the incubation medium with the U87 glioblastoma cells, advancing identification of any specific VC as responsible for the cytotoxicity observed would be mainly speculation. However, considering the reported effects of POVs on CHO cells growth inhibition [62] the possible stabilization of PV14 anions by BSA present in the incubation media, and their redox properties, we may state that PV14 anions are among the stronger candidates as species initiating the cytotoxic effects observed.

3. Conclusion

A POV hybrid, based on phosphotetradecavanadate anions and benzylammonium cations, was synthesized in acidic media and formulated as $(C_7H_{10}N)_6[H_3PV_{14}O_{42}]\bullet 7H_2O$. The crystal structure revealed that the compound displays a supramolecular 3D architecture established by hydrogen-bonding interactions involving the organic cations, hydration water molecules and surface POV O-atoms. The FTIR and PXRD spectroscopic results are in accordance with the single-crystal X-ray results. Non-covalent interactions, such as H-bonding, were instrumental in stabilizing the 3D hybrid structure, which is in close accord with the Hirshfeld surface analysis. Cyclic voltammetry electrochemical studies indicate that the redox waves of PV14 compounds involve multi-electron processes. Computational studies of the electronic structure of PV14 anions confirm that in aqueous acidic conditions the protonation state can comprise 2, 3, 4 or 5 protons. The precise location of the protonation sites was identified and the progressive stabilization of the molecular orbitals by protonation was demonstrated. Additionally, the calculations confirmed the inherent tendency of the PV14 anions to accept several electrons at sufficiently low pH values, hence the propensity for formation of reduced forms and appearance of multi-electron redox waves at negative electrode potentials. The tendency to bind several protons yielding $[H_xPV_{14}O_{42}]^{(9-x)-}$ POVs and to form mixed-valence species are characteristics of PV14 compounds that are relevant for their biological effects. Furthermore, molecular dynamics calculations indicate that aggregation between PV14 units in aqueous solution can be ruled out, and just a moderate interaction between PV14 species and the benzylammonium counter cations is expected.

^{51}V NMR spectra recorded at pH ~2.5 with milimolar concentrations of the PV14 compounds demonstrate that they decompose slowly; in fact, only very minor peaks of decavanadate are detected after 24 h, demonstrating their kinetic stability. In contrast, at pH ~7 the PV14 species decompose quite fast. However, in similar conditions but in the presence of human serum albumin, the ^{51}V NMR bands due to PV14 anions broaden significantly, demonstrating rather strong interactions between the POVs and HSA, and their decomposition becomes much slower.

The compound formulated as $(NH_4)_6[H_3PV_{14}O_{42}]\bullet 19H_2O$ (**5**) also strongly inhibited the growth of glioblastoma U87 cells by triggering their apoptosis. In contrast, benzylamine alone was not cytotoxic against these cells. The vanadium species responsible for the biological effects observed could not be definitively identified, but it is reasonable to state

that PV14 anions were at least partly responsible for the observed biological effects.

4. Experimental section

4.1. Materials and methods

All chemicals were obtained from commercial sources and used without further purification. Carbon, hydrogen, and nitrogen were determined on a Perkin-Elmer 2400 CHN analyzer. FTIR spectra were obtained on a Bruker Alpha P spectrometer, and the electrochemical measurements were carried out on a CHI 660B electrochemical analyzer at room temperature. For the cyclic voltammetry (CV) measurements, a three-electrode electrochemical cell was used with platinum as the working electrode, platinum gauze as the counter electrode and a saturated calomel electrode (SCE) as reference electrode.

The solution speciation diagrams were calculated using the computer program HYSS [111]. This computer program may be downloaded free of charge from the internet. The formation constants used are from [86,109,112]. In this work the equilibria are written considering the components H^+, $H_2VO_4^-$, and $H_2PO_4^-$, and the complexes are formed according to eqn:

$$pH^+ + q\ H_2VO_4^- + s\ H_2PO_4^- \leftrightarrows (H^+)p\ (H_2VO_4^-)q\ (H_2PO_4^-)s^{\,p-q-s}.$$

Formation constants are thus denoted $\beta_{p,q,s}$, and vanadium and phosphorus containing species are given the notation $H_pP_sV_qO_n$, including an adequate number of O atoms.

The biological data were analyzed by Graphpad prizm 8 software using Anova one-way Tukey's multiple comparison test. Results are represented as mean ± SD and P value <0.05 was considered statistically significant (* $p < 0.05$; *** $p < 0.001$ and **** $p < 0.0001$).

4.2. Synthetic procedure

Compound ***1***. In a small vial, a suspension containing 4.75 mmoles (0.556 g) of NH_4VO_3, 1.19 mmoles (0.297 g) of $CuSO_4{\cdot}5H_2O$ and 1.25 mmoles (0.144 g) of $NH_4H_2PO_4$ in ca. 30 mL of H_2O, adjusted to pH = 3.7 by nitric acid (2 M), was left to reflux at 90 °C for 40 min. Then, 0.0457 mol of benzylamine ($C_6H_5CH_2NH_2$) were added dropwise to the mixture, which was then left under reflux for additional 4 h. The mixture was allowed to cool down to room temperature and any solid product was filtered out. The solvent was removed under vacuum and the resulting solid recrystallized in MeOH. Brown crystals suitable for single-crystal X-ray diffraction analyses were isolated after the slow evaporation of the final solution at room temperature. Yield: 0.375 g, 0.171 mmole (50.4 % based on V). Elemental analysis for $C_{42}H_{77}N_6O_{49}PV_{14}$ (M_r = 2194.22 g mol^{-1}): *Calc (%)* C, 22.96; H, 2.87; N, 3.82; *Found (%)* C, 22.85; H, 2.75; N, 3.91. FTIR (s = strong, m = medium, w = weak, br = broad): 3005(br), 2709(br), 2412(br), 1581(s), 1459(m), 1404(w), 1241(w), 1065(s), 938(s), 802(m), 717(m), 582(w), 509(m), Fig. S1.

Compound ***5***. Ammonium metavanadate (NH_4VO_3) (0.1169 g, 0.999 mmole) and ammonium dihydrogen phosphate ($NH_4H_2PO_4$) (0.2299 g, 2.00 mmoles) were dissolved in 30 mL hot water. The solution's pH was adjusted to 2.2 by adding sulfuric acid at 60 °C. After 20 min NH_4Cl (0.02674 g, 0.500 mmole) was added to this solution. The mixture was left under reflux for around 3 h and then it was allowed to cool down to room temperature. After ~24 h the solid product was filtered out. Yield: 0.115 g, 6.15×10^{-2} mmole (86.1 % based on V). Elemental analysis for $C_0H_{65}N_6O_{60}PV_{14}$ (M_r = 1870 g mol^{-1}): *Calc (%)* C, 0; H, 3.48; N, 4.50; *Found (%)* C, 0.02; H, 3.25; N, 4.57.

4.3. Single-crystal X-ray crystallography

Crystallographic data for compound **1** are summarized in Table 3. Intensity data were collected at 100(2) K on an Agilent Technologies SuperNova diffractometer equipped with monochromated Mo Kα radiation (λ = 0.71073 Å) and an Hybrid Pixel Array detector. Data frames were processed (unit cell determination, multi-scan absorption correction, intensity data integration and correction for Lorentz and polarization effects using the CrysAlis Pro software package [133]. The structure was solved using OLEX2 [134] and refined by full-matrix least squares with SHELXL-2018/9 [135]. Final geometrical calculations were carried out with PLATON [136] as integrated in WinGX [137]. Thermal vibrations were treated anisotropically for all non-H atoms in both compounds. Hydrogen atoms of the organic ligands were placed in calculated positions and refined using a riding model with standard SHELXL parameters. Protonation sites from POV O-atoms in 1 were located in the Fourier map, in good agreement with BVS calculations. Seven positions suitable for water molecules of hydration were located on the Fourier map of 1, and their occupancy was initially refined without restrictions. These occupancies were rounded to the first decimal in the last refinement cycle. Molecular graphics were made using Diamond 3.2.

Table 3
Experimental details for the X-ray diffraction study and crystal data *for 1*.

Empirical formula	$(C_7H_{10}N)_6[H_3PV_{14}O_{42}]\bullet 7H_2O$
Formula weight (g.mol^{-1})	2194.19
Temperature	170 K
Crystal system	Monoclinic
Space group	$P2_1/n$
A	18.7299 (3) Å
B	11.3011 (2) Å
C	35.8837 (5) Å
A	90°
B	95.519 (1)°
Γ	90°
V	7560.2 (2)
Z	4
μ	1.77 mm
F(000)	4396
Index ranges	$-25 \le h \le 24$;$-15 \le k \le 15$; $-50 \le l \le 45$
Radiation	Mo Kα(λ = 0.71073)
Reflections collected	19,001
Independent reflections	19,001
R_{int}	0.039
Reflections with $I > 2\sigma(I)$	14,965
Refined parameters	1014
S (goodness-of-fit)	1.04
Final R indexes [$I \geq 2\sigma(I)$]	$R_1 = 0.032$, $wR_2 = 0.087$
$\Delta\rho_{max}/\Delta\rho_{min}$	1.15 eÅ^{-3}/−0.66 eÅ^{-3}

CCDC 2253859 (compound **1**) contains the supplementary crystallographic data for the structure reported in this paper. These data can be obtained free of charge via http://www.ccdc.cam.ac.uk/conts/retrieving.html or from the Cambridge Crystallographic Data Centre, 12 Union Road, Cambridge CB2 1EZ, UK; fax: (+44) 1223 336,033; or e-mail: deposit@ccdc.cam.ac.uk. Supplementary data associated with this article may be found, in the online version, at Doi: $$$$$.

4.4. Viability assay

U87 human glioblastoma cancer cells were generously provided by Pr. José Luis from Neurophysiopathology Institute, University of Aix Marseille. Cells were cultured daily on Dulbecco's Modified Medium (DMEM) (Gibco™, Sigma) supplemented with 10 % fetal bovine serum (FBS), antibiotic mixture (100 μg/mL) and L-glutamine (100 μg/mL) then placed in incubator with 5 % of CO_2 at 37 °C. U87 cells were seeded on 96 wells plate at 10^4 cells per well and incubated for 18 h. Subsequently, cells were treated with different doses of compounds and incubated for 24 h or 72 h. Then, 100 μL/well of MTT (3-(4,5-dimethylthiazol-2-yl)-2, 5-diphenyltetrazolium bromide) solution (0.5 mg/mL) was added and cells were incubated for another 3 h at 37 °C. After the transformation of MTT on formazan, 100 μL of DMSO was added to each sample and the optical density DO was measured at 560 nm.

4.5. Apoptosis-induced detection

The pro-apoptosis effect of compound **1** was evaluated using the RealTimeGlo™ Annexin V Apoptosis and Necrosis Kit (Promega). Cells (at 10^4 cells per well) were seeded in 100 μL medium and incubated overnight. Three concentrations of **1** corresponding to the IC_{50}, ½ IC_{50} and 2xIC_{50} of viability, were used. H_2O_2 (200 μM) was used as positive control for apoptosis and necrosis at 200 μM and cells were incubated for 24 h at 37°. Luminescence and fluorescence (Excitation 485 nm, Emission 525–530 nm) were then measured.

4.6. Computational details

4.6.1. DFT calculations

We fully optimized the structures of the tetradecavanadate polyoxovanadate for different degrees of protonation at the DFT level, as implemented in ADF 2019.3 package,[138] using the hybrid functional PBE0 [138–140] and a TZ2P Slater basis set. The solvent effects, necessary when comparing systems carrying different molecular charges, were included via the conductor-like screening model (COSMO) with ε = 78.39 for water [141]. The scalar relativistic effects via the zeroth-order regular approximation (ZORA) were included to electrons [142]. No imaginary frequencies were found after optimization of the fully deprotonated $[PV_{14}O_{42}]^{9-}$ structure, validating it as a real minimum. A data set of the collection of computational results is available in the ioChem-BD repository [143] accessible via doi: 10.19061/iochem-bd-2-61. For the determination of accurate protonation energies, we computed several water clusters with and without a hydronium molecule, i.e. $(H_2O)_nH_3O^+$ and $(H_2O)_n$ (n = 11–20), and their associated energies, to be applied in protonation reaction calculations as previously done in ref. [87].

4.6.2. Molecular dynamics

We carried out atomistic molecular dynamics (MD) simulations with explicit solvent molecules to determine the benzylammonium cation distribution around the POMs in water, using the GROMACS 2019.3 [144] code and a modified AMBER 99 Force Field [145] which has been satisfactorily employed to study the aggregation of POMs in different environments [146]. The force field provides the potential energy of the system as the sum of bond, angle and dihedral deformation energies, and non-bonding terms. The latter consist of pairwise additive electrostatic and van der Waals potentials, described by a 1–6-12 Lennard-Jones function, which accounts for interactions between atoms that are separated by more than three bonds, or non-bonded at all. For Coulombic interactions, we applied a cutoff of 10 Å, corrected for long-range electrostatics by using the particle-particle mesh Ewald (PKME) summation method. Bonds involving H atoms were restrained by the LINCS algorithm. For van der Waals interactions we applied an atom cutoff of 14 Å, and we set a 1–4 correction parameter to reduce the exaggeration of short-range interatomic repulsion caused by the LJ potential, specifying that contributions from pairs of atoms connected by three bonds are modified by the 1–4 factor. The force-field parameters for the POV were obtained from the work by López et al. [147] and the TIP3P model [148] to describe solvent water molecules. We used CHelpG atomic charges derived from the electrostatic potential obtained with the Gaussian16 package [149] at the DFT level using B3LYP functional and a 6–31 + G* Pople atomic basis set for O-atoms and a LANL2DZ(f) atomic basis set for all the others. The MD trajectories were obtained under 3D-periodic boundary conditions with a fundamental cubic box of 8.06 nm side (~424 $Å^3$ volume) containing five POM units, the number of benzylammonium cations required to neutralize the system, and water molecules as solvent for a [PV14] = 16 mM. Production runs were performed within a canonical (*NVT*) ensemble during 20 ns, collecting data at 1 ps steps. All simulations were carried out at 300 K, controlling the temperature by coupling the system to a thermal bath using the velocity-rescaling algorithm. Before production runs, all systems were equilibrated by an initial 500 ps run at constant *NVT*, followed by a 1 ns run at constant *NPT* to readjust the box size and a final 500 ps run at constant *NVT*. Production trajectories simulate 20 ns with a canonical (*NVT*) ensemble, with data collected every 1 ps.

Author statements

AI statement: In no part of the preparation or writing of the present manuscript was AI softwwre used.

CRediT authorship contribution statement

Rim Zarroug: Writing – original draft, Resources, Methodology, Investigation, Formal analysis, Data curation. **Wassim Moslah:** Writing – original draft, Validation, Methodology, Investigation, Formal analysis, Data curation. **Najet Srairi-Abid:** Writing – original draft, Validation, Resources, Methodology, Investigation, Funding acquisition, Formal analysis, Data curation, Conceptualization. **Beñat Artetxe:** Writing – original draft, Validation, Resources, Methodology, Formal analysis. **Albert Masip-Sánchez:** Writing – original draft, Investigation, Formal analysis, Data curation. **Xavier López:** Writing – review & editing, Writing – original draft, Visualization, Validation, Supervision, Resources, Project administration, Investigation, Formal analysis, Data curation, Conceptualization. **Brahim Ayed:** Writing – original draft, Validation, Methodology, Investigation, Formal analysis, Data curation. **Nádia Ribeiro:** Writing – original draft, Methodology, Formal analysis, Data curation. **Isabel Correia:** Writing – original draft, Validation, Methodology, Investigation, Formal analysis, Data curation, Conceptualization. **Leonor Corte-Real:** Validation, Methodology, Investigation, Formal analysis, Data curation. **João Costa Pessoa:** Writing – review & editing, Writing – original draft, Visualization, Validation, Supervision, Resources, Project administration, Methodology, Investigation, Funding acquisition, Formal analysis, Data curation, Conceptualization.

Declaration of competing interest

There were no financial or personal relationships that may be perceived as influencing the work now submitted.

João Costa Pessoa.

Acknowledgements

This work was supported by *Fundação para a Ciência e a Tecnologia* (FCT) [projects' numbers UIDB/00100/2020 (doi: 10.54499/UIDB/00100/2020), UIDP/00100/2020 (doi: 10.54499/UIDP/00100/2020) and LA/P/0056/2020 (doi: 10.54499/LA/P/0056/2020)]. It was also supported by UPV/EHU and Gobierno Vasco [projects: EHU-N23/03, IT1722-22 and KK2024-00062], as well as, SGIker (UPV/EHU, ERDF, EU) [technical and human support], as well as by the Generalitat de Catalunya [project 2021SGR00110] and by the Spanish Government [grant PID2023-149905NB-I00, funded by MCIN/AEI/ 10.13039/501100011033]. W.M. and N.S.-A. also acknowledge the support of the Tunisian Ministry of Higher Education and Scientific Research [LR 20 IPT 01].

Appendix A. Supplementary data

Supplementary data to this article can be found online at https://doi.org/10.1016/j.jinorgbio.2025.112882.

Data availability

Provisional Statement: Crystallographic data for compound **1** was deposited at the CCDC database under the accession number 2253859 and can be obtained from https://www.ccdc.cam.ac.uk/structures/

The data will be made available after acceptance and publication by

the Journal.

The Open Access option will be used in the frame of the 2025–2027 Portugal Consortia FCCN b-on open access agreement with Elsevier.

Journal of Inorganic Biochemistry will provide a DOI for the publication.

We will comply with data-sharing policies once the paper is accepted.

Supplementary material will also be made available by the Journal.

Data supporting this study are not publicly available at this stage. In some restricted cases it will be shared upon reasonable request to the corresponding author.

João Costa Pessoa.

References

[1] M.T. Pope, Heteropoly and Isopoly Oxometalates, Springer-Verlag, New York, 1983, p. 58.

[2] M.T. Pope, A. Müller, Polyoxometalate chemistry: an old field with new dimensions in several disciplines, Angew. Chem. Int. Ed. 30 (1) (1991) 34–48, https://doi.org/10.1002/anie.199100341.

[3] Y. Hayashi, Hetero and lacunary polyoxovanadate chemistry: synthesis, reactivity and structural aspects, Coord. Chem. Rev. 255 (19–20) (2011) 2270–2280, https://doi.org/10.1016/j.ccr.2011.02.013.

[4] N.I. Gumerova, A. Rompel, Interweaving disciplines to advance chemistry: applying polyoxometalates in biology, Inorg. Chem. 60 (9) (2021) 6109–6114, https://doi.org/10.1021/acs.inorgchem.1c00125.

[5] M.J.W. Budych, K. Staszak, A. Bajek, F. Pniewski, R. Jastrząb, M. Staszak, B. Tylkowski, K. Wieszczycka, The future of polyoxymetalates for biological and chemical apllications, Coord. Chem. Rev. 493 (2023) 215306, https://doi.org/10.1016/j.ccr.2023.215306.

[6] Y.G. Wei, Polyoxometalates: An interdisciplinary journal focused on all aspects of polyoxometalates, Polyoxometalates 1 (1) (2022) 9140014, https://doi.org/10.26599/POM.2022.9140014.

[7] X. Wang, S. Wei, C. Zhao, X. Li, J. Jin, X. Shi, Z. Su, J. Li, J. Wang, Promising application of polyoxometalates in the treatment of cancer, infectious diseases and Alzheimer's disease, J. Biol. Inorg. Chem. 27 (2022) 405–419, https://doi.org/10.1007/s00775-022-01942-7.

[8] S.M. Wang, J. Hwang, E. Kim, Polyoxometalates as promising materials for electrochromic devices, J. Mater. Chem. C 7 (2019) 7828–7850, https://doi.org/10.1039/C9TC01722D.

[9] S.S. Wang, G.Y. Yang, Hetero and lacunary polyoxovanadate chemistry: synthesis, reactivity and structural aspects, Chem. Rev. 115 (19–20) (2015) 4893–4962, https://doi.org/10.1016/j.ccr.2011.02.013.

[10] L. Al-Hussaini, S. Valange, M.E. Gálvez, F. Launay, Alternative ball-milling synthesis of vanadium-substituted polyoxometalates as catalysts for the aerobic cleavage of C–C and C–O bonds, Dalton Trans. 50 (2021) 12850–12859, https://doi.org/10.1039/D1DT01585K.

[11] J. Li, C. Wei, Y. Han, Y. Mei, X. Cheng, X. Huang, C. Hu, Triazole-directed fabrication of polyoxovanadate-based metal–organic frameworks as efficient multifunctional heterogeneous catalysts for the Knoevenagel condensation and oxidation of alcohols, Dalton Trans. 50 (2021) 10082–10091, https://doi.org/10.1039/D1DT01413G.

[12] X. Huang, X. Gu, H. Zhang, G. Shen, S. Gong, B. Yang, Y. Wang, Y. Chen, Decavanadate-based clusters as bifunctional catalysts for efficient treatment of carbon dioxide and simulant sulfur mustard, J. CO2 Util. 45 (2021) 101419, https://doi.org/10.1016/j.jcou.2020.101419.

[13] S.Y. Lai, K.H. Ng, C.K. Cheng, H. Nur, M. Nurhadi, M. Arumugam, Photocatalytic remediation of organic waste over Keggin-based polyoxometalate materials: a review, Chemosphere 263 (2021) 128–244, https://doi.org/10.1016/j.chemosphere.2020.128244.

[14] Y.F. Song, R. Tsunashima, Recent advances on polyoxometalate-based molecular and composite materials, Chem. Soc. Rev. 41 (22) (2012) 7384–7402, https://doi.org/10.1039/C2CS35143A.

[15] L.E. Van Gelder, E. Schreiber, E.M. Matson, Physicochemical implications of alkoxide "mixing" in polyoxovanadium clusters for nonaqueous energy storage, J. Mater. Chem. A 7 (9) (2019) 4893–4902, https://doi.org/10.1039/C8TA12306C.

[16] J. Lei, J.J. Yang, T. Liu, R.M. Yuan, D.R. Deng, M.S. Zheng, J.J. Chen, L. Cronin, Q.F. Dong, Tuning redox active Polyoxometalates for efficient Electron-coupled proton-buffer-mediated water splitting, Chem. Eur. J. 25 (49) (2019) 11432–11436, https://doi.org/10.1002/chem.201903142.

[17] J. Suárez-Guevara, V. Ruiz, P. Gomez-Romero, Hybrid energy storage: high voltage aqueous supercapacitors based on activated carbon–phosphotungstate hybrid materials, J. Mater. Chem. A 2 (4) (2014) 1014–1021, https://doi.org/10.1039/C3TA14455K.

[18] K.Yu. Monakhov, W. Bensch, P.K. Kögerler, Semimetal-functionalised polyoxovanadates, Chem. Soc. Rev. 44 (2015) 8443–8483, https://doi.org/10.1039/C5CS00531K.

[19] Y. Ji, X. Liu-Théato, Y. Xiu, S. Indris, C. Njel, J. Maibach, H. Ehrenberg, M. Fichtner, Z. Zhao-Karger, Polyoxometalate modified separator for performance enhancement of magnesium–sulfur batteries, Adv. Funct. Mater. 31 (26) (2021) 202100868, https://doi.org/10.1002/adfm.202100868.

[20] A. Xie, C.A. Ma, L. Wang, Y. Chu, $Li_6V_{10}O_{28}$, a novel cathode material for Li-ion battery, Electrochim. Acta 52 (9) (2007) 2945–2949, https://doi.org/10.1016/j.electacta.2006.08.069.

[21] M. Genovese, K. Lian, Polyoxometalate modified inorganic–organic nanocomposite materials for energy storage applications: a review, Curr. Opin. Solid State Mater. Sci. 19 (2) (2015) 126–137, https://doi.org/10.1016/j.cossms.2014.12.002.

[22] J. Friedl, M.V. Holland-Cunz, F. Cording, F. Pfanschilling, C. Wills, W. McFarlane, B. Schricker, R. Fleck, H. Wolfschmidt, U. Stimming, Asymmetric polyoxometalate electrolytes for advanced redox flow batteries, Energy Environ. Sci. 11 (10) (2018) 3010–3018, https://doi.org/10.1039/C8EE00422F.

[23] L. Lian, H. Zhang, S. An, W. Chen, Y.F. Song, Polyoxometalates-based heterogeneous catalysts in acid catalysis, Sci. China Chem. 64 (7) (2021) 1117–1130, https://doi.org/10.1007/s11426-020-9957-0.

[24] X. Zhong, Y. Lu, F. Luo, Y. Liu, X. Li, S. Liu, A nanocrystalline POM@ MOFs catalyst for the degradation of phenol: effective cooperative catalysis by metal nodes and POM guests, Chem. Eur. J. 24 (12) (2018) 3045–3051, https://doi.org/10.1002/chem.201705677.

[25] J. Ge, J. Hu, Y. Zhu, Z. Zeb, D. Zang, Z. Qin, Y. Huang, J. Zhang, Y. Wei, Recent advances in polyoxometalates for applications in electrocatalytic hydrogen evolution reaction, Acta Phys. -Chim. Sin. 36 (1) (2020) 1906063, https://doi.org/10.3866/PKU.WHXB201906063.

[26] J.D. Somasundaram, A. Ebrahimi, S.P. Nandan, A. Cherevan, D. Eder, M. Supolíková, E. Nováková, R. Gyepes, L. Krivosudský, Functionalization of decavanadate anion by coordination to cobalt(II): binding to proteins, cytotoxicity, and water oxidation catalysis, J. Inorg. Biochem. 239 (2023) 112067, https://doi.org/10.1016/j.jinorgbio.2022.112067.

[27] S. Treviño, A. Díaz, E. Sánchez-Lara, B.L. Sanchez-Gaytan, J.M. Perez-Aguilar, E. González-Vergara, Pharmacological aspects, and metabolic implications in diabetes mellitus, Biol. Trace Elem. Res. 188 (2019) 68–98, https://doi.org/10.1007/s12011-018-1540-6.

[28] J. Costa Pessoa, S.B. Etcheverry, D. Gambino, Coord, Chem. Rev. 301-302 (2025) 24–48, https://doi.org/10.1016/j.ccr.2014.12.002.

[29] E. Kioseoglou, S. Petanidis, C. Gabriel, A. Salifoglou, The chemistry and biology of vanadium compounds in cancer therapeutics, Coord. Chem. Rev. 301-302 (2025) 87–105, https://doi.org/10.1016/j.ccr.2015.03.010.

[30] J.L. Domingo, M. Gomez, Vanadium compounds for the treatment of human diabetes mellitus: a scientific curiosity? A review of thirty years of research, Food Chem. Toxicol. 95 (2016) 137–141, https://doi.org/10.1016/j.fct.2016.07.005.

[31] T. Scior, J.A. Guevara-Garcia, Q.-T. Doc, P. Bernard, S. Laufer, Why antidiabetic vanadium complexes are not in the pipeline of "big pharma" drug research? A critical review, Curr. Med. Chem. 23 (25) (2016) 2874–2891, https://doi.org/10.2174/0929867323666160321121138.

[32] D. Rehder, The potentiality of vanadium in medicinal applications, Inorg. Chim. Acta 504 (2020) 119445, https://doi.org/10.1016/j.ica.2020.119445.

[33] D. Rehder, Vanadium in biological systems and medicinal applications, Inorg. Chim. Acta 549 (2023) 121387, https://doi.org/10.1016/j.ica.2023.121387.

[34] D.C. Crans, L. Henry, G. Cardiff, B.I. Posner, Essential metals in medicine: therapeutic use and toxicity of metal ions in the clinic, Met. Lons Life Sci. 19 (2019) 203–230, https://doi.org/10.1515/9783110527872.

[35] M. Aureliano, N.I. Gumerova, G. Sciortino, E. Garribba, A. Rompel, D.C. Crans, Polyoxovanadates with emerging biomedical activities, Coord. Chem. Rev. 447 (2021) 214143, https://doi.org/10.1016/j.ccr.2021.214143.

[36] D.C. Crans, J.J. Smee, E. Gaidamauskas, L. Yang, The chemistry and biochemistry of vanadium and the biological activities exerted by vanadium compounds, Chem. Rev. 104 (2004) 849–902, https://doi.org/10.1021/cr020607t.

[37] R. Dinda, E. Garribba, D. Sanna, D.C. Crans, J. Costa Pessoa, Hydrolysis, Ligand exchange and redox properties of vanadium compounds: implications of solution transformation on biological, Chem. Rev. 125 (2025) 1468–1603, https://doi.org/10.1021/acs.chemrev.4c00475.

[38] T.M. McAusland, J.P. van Vloten, L.A. Santry, M.M. Guilleman, A.D. Rghei, E. M. Ferreira, J.C. Ingrao, R. Arulanandam, P.P. Major, L. Susta, K. Karimi, J. S. Diallo, B.W. Bridle, S.K. Wootton, Combining vanadyl sulfate with Newcastle disease virus potentiates rapid innate immune-mediated regression with curative potential in murine cancer models, Mol. Ther. Oncolyt. 20 (2021) 306–324, https://doi.org/10.1016/j.omto.2021.01.009.

[39] I. Werner, J. Griebel, A. Masip-Sánchez, X. López, K. Załęski, P. Kozłowski, A. Kahnt, M. Boerner, Z. Warneke, J. Warneke, S. Soni, R.C. Chiechi, K. Yu. Monakhov, Hybrid molecular magnets with lanthanide- and countercation-mediated interfacial electron transfer between phthalocyanine and polyoxovanadate, Inorg. Chem. 62 (9) (2023) 3761–3775, https://doi.org/10.1021/acs.inorgchem.2c03599.

[40] M. Moors, J. Warneke, M. Glöß, X. López, C. de Graaf, B. Abel, K.Yu. Monakhov, Insights from adsorption and Electron modification studies of Polyoxometalates on surfaces for molecular memory applications, Acc. Chem. Res. 54 (17) (2021) 3377–3389, https://doi.org/10.1021/acs.accounts.1c00311.

[41] A. Notario-Estévez, P. Kozłowski, O. Linnenberg, C. de Graaf, X. López, K. Yu. Monakhov, Decoding the role of encapsulated ions in the electronic and magnetic properties of mixed-valence polyoxovanadate capsules $\{X@V_{22}O_{54}\}$ ($X = ClO_4^-$, SCN^-, $VO_2F_2^-$): a combined theoretical approach, Phys. Chem. Chem. Phys. 20 (26) (2018) 17847–17858, https://doi.org/10.1039/C8CP02669F.

[42] O. Linnenberg, M. Moors, A. Notario-Estévez, X. López, C. de Graaf, S. Peter, C. Bäumer, R. Waser, K.Yu. Monakhov, Addressing multiple resistive states of polyoxovanadates: conductivity as a function of individual molecular redox states, J. Am. Chem. Soc. 140 (48) (2018) 16635–16640, https://doi.org/10.1021/jacs.8b08780.

[43] O. Linnenberg, M. Moors, A. Solé-Daura, X. López, C. Bäumer, E. Kentzinger, W. Pyckhout-Hintzen, K.Yu. Monakhov, Molecular characteristics of a mixed-valence polyoxovanadate $\{V_{18}^{IV/V}O_{42}\}$ in solution and at the liquid–surface interface, J. Phys. Chem. C 121 (19) (2017) 10419–10429, https://doi.org/10.1021/acs.jpcc.7b02138.

[44] D.C. Crans, J.J. Smee, E. Gaidamauskas, L. Yang, The chemistry and biochemistry of vanadium and the biological activities exerted by vanadium compounds, Chem. Rev. 104 (2) (2004) 849–902, https://doi.org/10.1021/cr020607t.

[45] J. Costa Pessoa, E. Garribba, M.F.A. Santos, T. Santos-Silva, Vanadium and proteins: uptake, transport, structure, activity and function, Coord. Chem. Rev. 301-302 (2015) 49–86, https://doi.org/10.1016/j.ccr.2015.03.016.

[46] S. Trevino, A. Diaz, E. Sanchez-Lara, B.L. Sanchez-Gaytan, J.M. Perez-Aguilar, E. Gonzalez-Vergara, Vanadium in biological action: chemical, pharmacological aspects, and metabolic implications in diabetes mellitus, Biol. Trace Elem. Res. 188 (2019) 68–98, https://doi.org/10.1007/s12011-018-1540-6.

[47] M.M. Altaf, X.-P. Diao, A. Rehman, M. Imtiaz, A. Shakoor, M.A. Altaf, H. Younis, P. Fu, M.U. Ghani, Effect of vanadium on growth, photosynthesis, reactive oxygen species, antioxidant enzymes, and cell death of rice, J. Soil Sci. Plant Nutr. 20 (2020) 2643–2656, https://doi.org/10.1007/s42729-020-00330-x.

[48] S. Treviño, A. Diaz, Vanadium and insulin: partners in metabolic regulation, J. Inorg. Biochem. 208 (2020) 111094, https://doi.org/10.1016/j.jinorgbio.2020.111094.

[49] T.C. Delgado, A.I. Tomaz, I. Correia, J. Costa Pessoa, J.G. Jones, C.F.G. G. Geraldes, M.M.C.A. Castro, Uptake and metabolic effects of insulin mimetic oxovanadium compounds in human erythrocytes, J. Inorg. Biochem. 99 (12) (2005) 2328–2339, https://doi.org/10.1016/j.jinorgbio.2005.08.014.

[50] H. Faneca, V.A. Figueiredo, A.I. Tomaz, G. Gonçalves, F. Avecilla, M.C. Pedroso de Lima, C.F.G.C. Geraldes, J. Costa Pessoa, M.M.C.A. Castro, Vanadium compounds as therapeutic agents: some chemical and biochemical studies, J. Inorg. Biochem. 103 (4) (2009) 601–608, https://doi.org/10.1016/j.jinorgbio.2008.11.004.

[51] G. Fraqueza, C.A. Ohlin, W.H. Casey, M. Aureliano, Sarcoplasmic reticulum calcium ATPase interactions with decaniobate, decavanadate, vanadate, tungstate and molybdate, J. Inorg. Biochem. 107 (1) (2012) 82–89, https://doi.org/10.1016/j.jinorgbio.2011.10.010.

[52] D.W. Boyd, K. Kustin, M. Niw, Do vanadate polyanions inhibit phosphotransferase enzymes? Biochim. Biophys. Acta Protein Struct. Mol. Enzymol. 827 (3) (1985) 472–475, https://doi.org/10.1016/0167-4838(85)90235-3.

[53] M.P.M. Marques, D. Gianolio, S. Ramos, L.A.E. Batista de Carvalho, M. Aureliano, An EXAFS approach to the study of polyoxometalate–protein interactions: the case of decavanadate–actin, Inorg. Chem. 57 (18) (2017) 10893–10903, https://doi.org/10.1021/acs.inorgchem.7b01018.

[54] M. Aureliano, N.I. Gumerova, G. Sciortino, E. Garribba, C.C. McLauchlan, A. Rompel, D.C. Crans, Polyoxidovanadates' interactions with proteins: an overview, Coord. Chem. Rev. 454 (2022) 214–344, https://doi.org/10.1016/j.ccr.2021.214344.

[55] G. Tito, G. Ferraro, F. Pisanu, E. Garribba, A. Merlino, Non-covalent and covalent binding of new mixed-valence cage-like polyoxidovanadate clusters to lysozyme, Angew. Chem. Int. Ed. 63 (31) (2024) e202406669, https://doi.org/10.1002/anie.202406669.

[56] K. Dan, K. Fujinami, H. Sumitomo, Y. Ogiwara, S. Suhara, Y. Konno, M. Sawada, Y. Soga, A. Takada, K. Takanashi, K. Watanabe, T. Shinozuka, Application of antiviral polyoxometalates to living environments—antiviral moist hand towels and stationery items, Appl. Sci. 10 (22) (2020) 82–146, https://doi.org/10.3390/app10228246.

[57] M. Aureliano, The future is bright for Polyoxometalates, BioChem 2 (1) (2022) 8–26, https://doi.org/10.3390/biochem2010002.

[58] M.F.A. Santos, J. Costa Pessoa, Interaction of vanadium complexes with proteins: revisiting the reported structures in the protein data Bank (PDB) since 2015, Molecules 28 (18) (2023) 6538, https://doi.org/10.3390/molecules28186538.

[59] X. Xu, N. Bosnjakovic-Pavlovic, M.B. Colovic, D.Z. Krstic, V.M. Vasic, J.M. Gillet, P.F. Wu, Y.G. Wei, A. Spasojevic-de Biré, A combined crystallographic analysis and *ab initio* calculations to interpret the reactivity of functionalized hexavanadates and their inhibitor potency toward Na^+/K^+-ATPase, J. Inorg. Biochem. 161 (2016) 27–36, https://doi.org/10.1016/j.jinorgbio.2016.04.029.

[60] C. Amante, D. Sousa-Coelho, A. Luisa, M. Aureliano, Vanadium and Melanoma: a systematic review, Metals 11 (5) (2021) 828, https://doi.org/10.3390/met11050828.

[61] L. García-García, F.J. Noriega, M.E. Meléndez-Bustamante, M.E. Castro, B. L. Sánchez-Gaytán, D. Choquesillo-Lazarte, E. González-Vergara, A. Rodríguez-Diéguez, 2-Aminopyrimidinium decavanadate: experimental and theoretical characterization, molecular docking, and potential antineoplastic activity, Inorganics 9 (9) (2021) 67, https://doi.org/10.3390/inorganics9090067.

[62] D. Althumairy, K. Postal, B.G. Barisas, G.G. Nunes, D.A. Roess, D.C. Crans, Polyoxometalates function as indirect activators of a G protein-coupled receptor, Metallomics 12 (7) (2020) 1044–1061, https://doi.org/10.1039/d0mt00044b.

[63] R. Dridi, Z. Abdelkafi-Koubaa, N. Srairi-Abid, B. Socha, M.F. Zid, One-pot synthesis, structural investigation, antitumor activity and molecular docking approach of two decavanadate compounds, J. Inorg. Biochem. 255 (2024) 112533, https://doi.org/10.1016/j.jinorgbio.2024.112533.

[64] S. Kowalski, D. Wyrzykowski, I. Inkielewicz-Stępniak, Molecular and cellular mechanisms of cytotoxic activity of vanadium compounds against cancer cells, Molecules 25 (7) (2020) 1757, https://doi.org/10.3390/molecules25071757.

[65] Y. Zhang, L. Wang, K. Zeng, K. Wang, X., Yang Vanadyl complexes discriminate between neuroblastoma cells and primary neurons by inducing cell-specific apoptotic pathways, J. Inorg. Biochem. 188 (2018) 76–87, https://doi.org/10.1016/j.jinorgbio.2018.08.005.

[66] D.C. Crans, L. Yang, A. Haase, X. Yang, Metallo-drugs: development and action of anticancer agents, Met. Lons Life Sci. 18 (2018) 251–279, https://doi.org/10.1515/9783110470734.

[67] M.S. Islas, L.G. Naso, L. Lezama, M. Valcarcel, C. Salado, M. Roura-Ferrer, E. G. Ferrer, P.A.M. Williams, Insights into the mechanisms underlying the antitumor activity of an oxidovanadium(IV) compound with the antioxidant naringenin. Albumin binding studies, J. Inorg. Biochem. 149 (2015) 12–24, https://doi.org/10.1016/j.jinorgbio.2015.04.011.

[68] Q.T. Ostrom, G. Cioffi, K. Waite, C. Kruchko, J.S. Barnholtz-Sloan, CBTRUS statistical report: primary brain and other central nervous system tumors diagnosed in the United States in 2014–2018, J. Neuro-Oncol. 23 (Supplement_3) (2021) iii1–iii105, https://doi.org/10.1093/neuonc/noab200.

[69] P. Wesseling, D. Capper, WHO 2016 classification of gliomas, Neuropathol. Appl. Neurobiol. 44 (2) (2018) 139–150, https://doi.org/10.1111/nan.12432.

[70] R. Davis, C. Weisbeck, Creating a supportive environment using cues for wayfinding in dementia, J. Gerontol. Nurs. 42 (3) (2016) 36–44, https://doi.org/10.3928/00989134-20160212-07.

[71] F.A. Mansouri, E. Koechlin, M.G. Rosa, M.J. Buckley, Managing competing goals — a key role for the frontopolar cortex, Nat. Rev. Neurosci. 18 (2017) 645–657, https://doi.org/10.1038/nrn.2017.111.

[72] R. Stupp, M. Gander, S. Leyvraz, E. Newlands, Current and future developments in the use of temozolomide for the treatment of brain tumours, Lancet Oncol. 2 (9) (2001) 552–560, https://doi.org/10.1016/S1470-2045(01)00489-2.

[73] T. Jiang, Y. Mao, W. Ma, Q. Mao, Y. You, X. Yang, C. Jiang, C. Kang, X. Li, L. Chen, X. Qiu, W. Wang, W. Li, Y. Yao, S. Li, S. Li, A. Wu, K. Sai, H. Bai, G. Li, B. Chen, K. Yao, X. Wei, X. Liu, Z. Zhang, Y. Dai, S. Lv, L. Wang, Z. Lin, J. Dong, G. Xu, X. Ma, J. Cai, W. Zhang, H. Wang, L. Chen, C. Zhang, P. Yang, W. Yan, Z. Liu, H. Hu, J. Chen, Y. Liu, Y. Yang, Z. Wang, Z. Wang, Y. Wang, G. You, L. Han, Z. Bao, Y. Liu, Y. Wang, X. Fan, S. Liu, X. Liu, Y. Wang, Q. Wang, CGCG clinical practice guidelines for the management of adult diffuse gliomas, Cancer Lett. 375 (2) (2016) 263–273, https://doi.org/10.1016/j.canlet.2016.01.024.

[74] N. Singh, A. Miner, L. Hennis, S. Mittal, Mechanisms of temozolomide resistance in glioblastoma - a comprehensive review, Cancer Drug Resist 4 (1) (2021) 17–43, https://doi.org/10.20517/cdr.2020.79.

[75] A. Arora, K. Somasundaram, Glioblastoma vs temozolomide: can the red queen race be won? Cancer Biol. Ther. 20 (8) (2019) 1083–1090, https://doi.org/10.1080/15384047.2019.1599662.

[76] Y. Yan, Z. Xu, S. Dai, L. Qian, L. Sun, Z. Gong, Targeting autophagy to sensitive glioma to temozolomide treatment, J. Exp. Clin. Cancer Res. 35 (2016) 23, https://doi.org/10.1186/s13046-016-0303-5.

[77] M.M. Mrugala, M.C. Chamberlain, Mechanisms of disease: temozolomide and glioblastoma—look to the future, Nat. Clin. Pract. Oncol. 5 (2008) 476–486, https://doi.org/10.1038/ncponc1155.

[78] A. Levina, G. Scalese, D. Gambino, D.C. Crans, P.A. Lay, Solution chemistry and anti-proliferative activity against glioblastoma cells of a vanadium(V) complex with two bioactive ligands, Front. Chem. Biol. Sec. Bioinorg. Chem. 3 (2024) 1394645, https://doi.org/10.3389/fchbi.2024.1394645.

[79] S. Xu, H. Liu, X. Li, J. Zhao, J. Wang, D.C. Crans, X. Yang, Approaches to selective and potent inhibition of glioblastoma by vanadyl complexes: inducing mitotic catastrophe and methuosis, J. Inorg. Biochem. 257 (2024) 112610, https://doi.org/10.1016/j.jinorgbio.2024.112610.

[80] C. Bates, K.L. Klugh, A.O. Galaeva, R.A. Patch, J.F. Manganaro, S.A. Markham, E. Scurek, A. Levina, P.A. Lay, D.C. Crans, Optimizing therapeutics for intratumoral cancer treatments: antiproliferative vanadium complexes in glioblastoma, Int. J. Mol. Sci. 26 (2025) 994, https://doi.org/10.3390/ijms26030994.

[81] K. Kostenkova, A. Levina, D. Walters, H.A. Murakami, P.A. Lay, D.C. Crans, Vanadium(V) pyridine-containing schiff base catecholate complexes are lipophilic, redox-active and selectively cytotoxic in glioblastoma (T98G) cells, Chem. Eur. J. 29 (68) (2023) e202302271, https://doi.org/10.1002/chem.202302271.

[82] H.A. Murakami, C. Uslan, A.A. Haase, J.T. Koehn, A.P. Vieira, D.J. Gaebler, J. Hagan, C.N. Beuning, N. Proschogo, A. Levina, P.A. Lay, D.C. Crans, Vanadium chloro-substituted schiff base catecholate complexes are reducible, lipophilic, water stable, and have anticancer activities, Inorg. Chem. 61 (2022) 20757–20773, https://doi.org/10.1021/acs.inorgchem.2c02557.

[83] A. Levina, C. Uslan, H. Murakami, D.C. Crans, P.A. Lay, Substitution kinetics, albumin and transferrin affinities, and hypoxia all affect the biological activities of anticancer vanadium(V) complexes, Inorg. Chem. 62 (43) (2023) 17804–17817, https://doi.org/10.1021/acs.inorgchem.3c02561.

[84] P. Nunes, I. Correia, I. Cavaco, F. Marques, T. Pinheiro, F. Avecilla, J. Costa Pessoa, Therapeutic potential of vanadium complexes with 1,10-phenanthroline ligands, *quo vadis*? Fate of complexes in cell media and cancer cells, J. Inorg. Biochem. 217 (2021) 111350, https://doi.org/10.1016/j.jinorgbio.2020.111350.

[85] G. Scalese, I. Machado, F. Salazar, E.L. Coitiño, I. Correia, J. Costa Pessoa, L. Pérez-Díaz, D. Gambino, Facing diseases caused by trypanosomatid parasites: rational design of multifunctional oxidovanadium(IV) complexes with bioactive ligands, Front. Chem. Biol. 2 (2024) 1304571, https://doi.org/10.3389/fchbi.2023.1304571.

[86] I. Andersson, A. Gorzsás, C. Kerezsi, I. Tóth, L. Pettersson, Speciation in the aqueous $H^+/H_2VO_4^-/H_2O_2$/phosphate system, Dalton Trans. 22 (2005) 3658–3666, https://doi.org/10.1039/B508273K.

[87] R. Zarroug, B. Artetxe, B. Ayed, X. López, N. Ribeiro, I. Correia, J. Costa Pessoa, New phosphotetradecavanadate hybrids: crystal structure, DFT analysis, stability

and binding interactions with bio-macromolecules, Dalton Trans. 51 (2022) 8303–8317, https://doi.org/10.1039/D2DT00690A.
[88] G. Fraqueza, J. Fuentes, L. Krivosudský, S. Dutta, S.S. Mal, A. Roller, G. Giester, A. Rompel, M. Aureliano, Inhibition of Na^+/K^+- and Ca^{2+}-ATPase activities by phosphotetradecavanadate, J. Inorg. Biochem. 197 (2019) 110700, https://doi.org/10.1016/j.jinorgbio.2019.110700.
[89] S. She, S. Bian, R. Huo, K. Chen, Z. Huang, J. Zhang, J. Hao, Y. Wei, Degradable organically-Derivatized Polyoxometalate with enhanced activity against glioblastoma cell line, Sci. Rep. 6 (2016) 33529, https://doi.org/10.1038/srep33529.
[90] R. Ksiksi, Z. Abdelkafi-Koubaa, S. Mlayah-Bellalouna, D. Aissaoui, N. Marrakchi, N. Srairi-Abid, M.F. Zid, M. Graia, Synthesis, structural characterization and antitumoral activity of $(NH_4)_4Li_2V_{10}O_{28}$. $10H_2O$ compound, J. Mol. Struct. 1229 (2021) 129–492, https://doi.org/10.1016/j.molstruc.2020.129492.
[91] M. Louati, R. Ksiksi, I. Elbini-Dhouib, S. Mlayah-Bellalouna, R. Doghri, N. Srairi-Abid, M.F. Zid, Synthesis, structure and characterization of a novel decavanadate, $Mg(H_2O)_6(C_4N_2H_7)_4V_{10}O_{28}{\cdot}4H_2O$, with a potential antitumor activity, J. Mol. Struct. 1242 (2021) 130711, https://doi.org/10.1016/j.molstruc.2021.130711.
[92] K. Nomiya, K. Kato, M. Miwa, Preparation and spectrochemical properties of soluble vanadophosphate polyanions with bicapped-Keggin structure, Polyhedron 5 (3) (1986) 811–813, https://doi.org/10.1016/S0277-5387(00)84442-3.
[93] M.T. Averbuch-Pouchot, A. Durif, Crystal structure of hexakis (ethanolammonium) decavanadate dihydrate, $(C_2H_8NO)_6(V_{10}O_{28})(H_2O)_2$, Zeitschrift für Kristallogr. – Cryst. Mat. 210 (1995) 156–157, https://doi.org/10.1524/zkri.1995.210.2.156.
[94] D. Corona-Motolinia Nidia, M. Valencia Beatriz, N. Lisset, L. Sánchez-Gaytán Brenda, J. Melendez Francisco, A. García-García, D. Choquesillo-Lazarte, A. Rodríguez-Diéguez, E. Castro María, E. González-Vergara, Tris(2-Pyridylmethylamine)$V(O)_2$ complexes as counter ions of diprotonated decavanadate anion: potential antineoplastic activity, Front. Chem. 10 (2022) 830511, https://doi.org/10.3389/fchem.2022.830511.
[95] E.J. Baran, C.I. Cabello, Vibrational and electronic spectra of the $PV_{14}O_{42}^{9-}$ polyanion, J. Mol. Struct. 174 (1988) 401–406, https://doi.org/10.1016/0022-2860(88)80191-1.
[96] R. Kato, A. Kobayashi, Y. Sasaki, The heteropolyvanadate of phosphorus. Crystallographic and NMR studies, Inorg. Chem. 21 (1) (1982) 240–246, https://doi.org/10.1021/ic00131a045.
[97] S. Uematsu, Z. Quan, Y. Suganuma, N. Sonoyama, Reversible lithium charge–discharge property of bi-capped Keggin-type polyoxovanadates, J. Power Sources 217 (2012) 13–20, https://doi.org/10.1016/j.jpowsour.2012.05.096.
[98] R.L. Meyer, R. Love, W.W. Brennessel, E.M. Matson, Mechanistic insights into polyoxometalate self-assembly in organic solvent: conversion of a cyclic polyoxovanadate-ethoxide to its Lindqvist congener, Chem. Commun. 56 (61) (2020) 8607–8610, https://doi.org/10.1039/D0CC03464A.
[99] Y. Kikukawa, K. Seto, S. Uchida, S. Kuwajima, Y. Hayashi, Solid-state umbrella-type inversion of a VO_5 square-pyramidal unit in a bowl-type Dodecavanadate induced by insertion and elimination of a guest molecule, Angew. Chem. Int. Ed. 57 (49) (2018) 16051–16055, https://doi.org/10.1002/anie.201809120.
[100] V. Rudnev, V.P. Morozova, T.A. Kaidalova, D.L. Boguta, P.S. Gordienko, The effect of Polyanions structure in the Bath on the composition of anodic-spark coatings, Prot. Met. 40 (2004) 204–205, https://doi.org/10.1023/B:PROM.0000021619.39732.6d.
[101] J. Friedl, F.L. Pfanschilling, M.V. Holland-Cunz, R. Fleck, B. Schricker, H. Wolfschmidt, U. Stimming, A polyoxometalate redox flow battery: functionality and upscale, Clean Energy 3 (4) (2019) 278–287, https://doi.org/10.1093/ce/zkz019.
[102] S. Nakamura, T. Yamawaki, K. Kusaka, T. Otsuka, T. Ozeki, Hydrogen-bond networks involving protonated Bicapped-Keggin Tetradecavanadophosphate anions, J. Clust. Sci. 17 (2006) 245–256, https://doi.org/10.1007/s10876-006-0064-y.
[103] W.H. Baur, The geometry of polyhedral distortions. Predictive relationships for the phosphate group, Acta Crystallogr. B30 (1974) 1195–1215, https://doi.org/10.1107/S0567740874004560.
[104] I.D. Brown, D. Altermatt, Bond-valence parameters obtained from a systematic analysis of the inorganic crystal structure database, Acta Crystallogr. Sect. B 41 (1985) 244–247, https://doi.org/10.1107/S0108768185002063.
[105] M. O'Keefe, N.E. Brese, Atom sizes and bond lengths in molecules and crystals, J. Am. Chem. Soc. 113 (9) (1991) 3226–3229, https://doi.org/10.1021/ja00009a002.
[106] R.C. Palenik, K.A. Abboud, G. Palenik, Bond valence sums and structural studies of antimony complexes containing Sb bonded only to O ligands, J. Inorg. Chim. Acta 358 (2005) 1034–1040, https://doi.org/10.1016/j.ica.2004.11.013.
[107] M.A. Spackman, D. Jayatilaka, Hirshfeld surface analysis, CrystEngComm 11 (2009) 19–32, https://doi.org/10.1039/B818330A.
[108] F.L. Hirshfeld, Bonded-atom fragments for describing molecular charge densities, Theor. Chim. Acta 44 (1977) 129–138, https://doi.org/10.1007/BF00549096.
[109] A. Selling, I. Andersson, L. Pettersson, C.M. Schramm, S.L. Downey, J.H. Grate, Multicomponent Polyanions, 47. The aqueous Vanadophosphate system, Inorg. Chem. 33 (14) (1994) 3141–3150, https://doi.org/10.1021/ic00092a021.
[110] S.C. Huang, C.C. Lin, C.W. Hu, Y.F. Liao, T.Y. Chen, H.Y. Chen, Vanadium-based polyoxometalate as electron/ion sponge for lithium-ion storage, J. Power Sources 435 (2019) 226702, https://doi.org/10.1016/j.jpowsour.2019.226702.
[111] L. Alderighi, P. Gans, A. Ienco, D. Peters, A. Sabatini, A. Vacca, Hyperquad simulation and speciation (HySS): a utility program for the investigation of equilibria involving soluble and partially soluble species, Coord. Chem. Rev. 184 (1) (1999) 311–318, https://doi.org/10.1016/S0010-8545(98)00260-4.
[112] L. Pettersson, I. Andersson, A. Gorzsas, Speciation in peroxovanadate systems, Coord. Chem. Rev. 237 (1–2) (2003) 77–87, https://doi.org/10.1016/S0010-8545(02)00223-0.
[113] J.M. Poblet, X. López, C. Bo, *Ab initio* and DFT modelling of complex materials: towards the understanding of electronic and magnetic properties of polyoxometalates, Chem. Soc. Rev. 32 (5) (2003) 297–308, https://doi.org/10.1039/B109928K.
[114] X. López, C. Bo, J.M. Poblet, Electronic properties of polyoxometalates: electron and proton affinity of mixed-addenda keggin and wells−dawson anions, J. Am. Chem. Soc. 124 (42) (2002) 12574–12582, https://doi.org/10.1021/ja020407z.
[115] A. Solé-Daura, A. Notario-Estévez, J.J. Carbó, J.M. Poblet, C. de Graaf, K. Y. Monakhov, X. López, How does the redox state of polyoxovanadates influence the collective behavior in solution? A case study with $[I@V_{18}O_{42}]^{q-}$ ($q = 3, 5, 7, 11$, and 13), Inorg. Chem. 58 (6) (2019) 3881–3894, https://doi.org/10.1021/acs.inorgchem.8b03508.
[116] H.A. Murakami, C. Uslan, A.A. Haase, J.T. Koehn, A.P. Vieira, D.J. Gaebler, J. Hagan, C.N. Beuning, N. Proschogo, A. Levina, P.A. Lay, D.C. Crans, Vanadium chloro-substituted schiff base catecholate complexes are reducible, lipophilic, water stable, and have anticancer activities, Inorg. Chem. 61 (51) (2022) 20757–20773, https://doi.org/10.1021/acs.inorgchem.2c02557.
[117] P. Nunes, I. Correia, F. Marques, A.P. Matos, M.M.C. Santos, C.G. Azevedo, J.-L. Capelo, H.M. Santos, S. Gama, T. Pinheiro, I. Cavaco, J. Costa Pessoa, Copper complexes with 1,10-Phenanthroline derivatives: underlying factors affecting their cytotoxicity, Inorg. Chem. 59 (13) (2020) 9116–9134, https://doi.org/10.1021/acs.inorgchem.0c00925.
[118] A. Levina, D.C. Crans, P.A. Lay, Speciation of metal drugs, supplements and toxins in media and bodily fluids controls *in vitro* activities, Coord. Chem. Rev. 352 (2017) 473–498, https://doi.org/10.1016/j.ccr.2017.01.002.
[119] A. Levina, P.A. Lay, Stabilities and biological activities of vanadium drugs: what is the nature of the active species? Chem. Asian J. 12 (14) (2017) 1692–1699, https://doi.org/10.1002/asia.201700463.
[120] G. Scalese, I. Correia, J. Benitez, S. Rostan, F. Marques, F. Mendes, A.P. Matos, J. Costa Pessoa, D. Gambino, Evaluation of cellular uptake, cytotoxicity and cellular ultrastructural effects of heteroleptic oxidovanadium (IV) complexes of salicylaldimines and polypyridyl ligands, J. Inorg. Biochem. 166 (2017) 162–172, https://doi.org/10.1016/j.jinorgbio.2016.11.010.
[121] D.C. Crans, B. Zhang, E. Gaidamauskas, A.D. Keramidas, G.R. Willsky, C. R. Roberts, Is vanadate reduced by thiols under biological conditions? Changing the redox potential of V(V)/V(IV) by complexation in aqueous solution, Inorg. Chem. 49 (2010) 4245–4256, https://doi.org/10.1021/ic100080k.
[122] D. Sanna, J. Palomba, G. Lubinu, P. Buglyo, S. Nagy, F. Perdih, E. Garribba, Role of ligands in the uptake and reduction of V(V) complexes in red blood cells, J. Med. Chem. 62 (2019) 654–664, https://doi.org/10.1021/acs.jmedchem.8b01330.
[123] I.G. Macara, K. Kustin, L.C. Cantley, Jr glutathione reduces cytoplasmic vanadate. Mechanism and physiological implications, Biochim. Biophys. Acta 629 (1980) 95–106, https://doi.org/10.1016/0304-4165(80)90268-8.
[124] J. Costa Pessoa, I. Tomaz, T. Kiss, E. Kiss, P. Buglyó, The systems $V^{IV}O^{2+}$-glutathione and related ligands: a potentiometric and spectroscopic study, J. Biol. Inorg. Chem. 7 (2002) 225–240, https://doi.org/10.1007/s007750100289.
[125] N. Ribeiro, I. Bulut, V. Pósa, B. Sergi, G. Sciortino, J. Costa Pessoa, L.B. Maia, V. Ugone, E. Garribba, É.A. Enyedy, C. Acilan, I. Correia, Solution chemical properties and anticancer potential of 8-hydroxyquinoline hydrazones and their oxidovanadium(IV) complexes, J. Inorg. Biochem. 235 (2022) 111932, https://doi.org/10.1016/j.jinorgbio.2022.111932.
[126] M. Fernández, L. Becco, I. Correia, J. Benítez, O.E. Piro, G.A. Echeverria, A. Medeiros, M. Comini, M.L. Lavaggi, M. González, H. Cerecetto, V. Moreno, J. Costa Pessoa, B. Garat, D. Gambino, Oxidovanadium(IV) and dioxidovanadium (V) complexes of tridentate salicylaldehyde semicarbazones: searching for prospective antitrypanosomal agents, J. Inorg. Biochem. 127 (2013) 150–160, https://doi.org/10.1016/j.jinorgbio.2013.02.010.
[127] I. Correia, N. Ribeiro, I. Bulut, B. Cevatemre, C. Teixeira, Y. Yildizhan, V. André, P. Adão, J. Costa Pessoa, C. Acilan, Cu(ii) and V(iv)O complexes with tri- or tetradentate ligands based on (2-hydroxybenzyl)-l-alanines reveal promising anticancer therapeutic potential, Dalton Trans. 50 (1) (2021) 157–169, https://doi.org/10.1039/D0DT03331F.
[128] S.S. Amin, K. Cryer, B. Zhang, S.K. Dutta, S.S. Eaton, O.P. Anderson, S.M. Miller, B.A. Reul, S.M. Brichard, D.C. Crans, Chemistry and insulin-mimetic properties of Bis(acetylacetonate)oxovanadium(IV) and derivatives, Inorg. Chem. 39 (3) (2000) 406–416, https://doi.org/10.1021/ic9905897.
[129] I. Correia, I. Chorna, I. Cavaco, S. Roy, M.L. Kuznetsov, N. Ribeiro, G. Justino, F. Marques, T. Santos Silva, M.F.A. Santos, H.M. Santos, J.L. Capelo, J. Doutch, J. Costa Pessoa, Interaction of $[V^{IV}O(acac)_2]$ with human serum transferrin and albumin, Chem. Asian J. 12 (16) (2017) 2062–2084, https://doi.org/10.1002/asia.201700469.
[130] E. Garribba, G. Micera, D. Sanna, The solution structure of bis(acetylacetonato) oxovanadium(IV), Inorg. Chim. Acta 359 (14) (2006) 4470–4476, https://doi.org/10.1016/j.ica.2006.05.028.
[131] G. Ferraro, G. Tito, G. Sciortino, E. Garribba, A. Merlino, Stabilization and binding of $[V_4O_{12}]^{4-}$ and unprecedented $[V_{20}O_{54}(NO_3)]^{n-}$ to lysozyme upon loss of ligands and oxidation of the potential drug $V^{IV}O$(acetylacetonato)$_2$, Angew. Chem. Int. Ed. 135 (50) (2023) e202310655, https://doi.org/10.1002/ange.202310655.
[132] G. Ferraro, M. Paolillo, G. Sciortino, F. Pisanu, E. Garribba, A. Merlino, Implications of protein interaction in the speciation of potential $V^{IV}O$–Pyridinone

drugs, Inorg. Chem. 62 (21) (2023) 8407–8417, https://doi.org/10.1021/acs.inorgchem.3c01041.
[133] CrysAlisPro Software System, Version 171.37.34 vol. 1, Agilent Technologies UK Ltd, Oxford, UK, 2014, 39.34.
[134] O.V. Dolomanov, L.J. Bourhis, R.J. Gildea, J.A.K. Howard, H. Puschmann, C13 (H13), C20 (H20), C10 (H10), C18 (H18), C11 (H11), C17 (H17) 3. b Idealised tetrahedral OH refined as rotating group: O5 (H5), O6 (H6), J. Appl. Crystallogr. 42 (2009) 339–341.
[135] G.M. Sheldrick, Crystal Structure Refinement with SHELXL. Acta Crystallogr, Sect. C: Struct. Chem. 71 (2015) 3–8, https://doi.org/10.1107/S2053229614024218.
[136] A.L. Spek, Structure validation in chemical crystallography, Acta Crystallogr. Sect. D: Biol. Crystallogr. D65 (2009) 148–155.
[137] L.J. Farrugia, *WinGX* suite for small-molecule single-crystal crystallography, J. Appl. Crystallogr. 32 (1999) 837–838, https://doi.org/10.1107/S0021889899006020.
[138] G. te Velde, F.M. Bickelhaupt, E.J. Baerends, C. Fonseca Guerra, S.J.A. van Gisbergen, J.G. Snijders, T. Ziegler, Chemistry with ADF, J. Comput. Chem. 22 (9) (2001) 931–967, https://doi.org/10.1002/jcc.1056.
[139] S. Grimme, Accurate description of van der Waals complexes by density functional theory including empirical corrections, J. Comput. Chem. 25 (12) (2004) 1463–1473, https://doi.org/10.1002/jcc.20078.
[140] M. Ernzerhof, G.E. Scuseria, Assessment of the Perdew–Burke–Ernzerhof exchange-correlation functional, J. Chem. Phys. 110 (11) (1999) 5029–5036, https://doi.org/10.1063/1.478401.
[141] C.C. Pye, T. Ziegler, An implementation of the conductor-like screening model of solvation within the Amsterdam density functional package, Theor. Chem. Accounts 101 (1999) 396–408, https://doi.org/10.1007/s002140050457.
[142] E. van Lenthe, A. Ehlers, E.J. Baerends, Geometry optimizations in the zero order regular approximation for relativistic effects, J. Chem. Phys. 110 (18) (1999) 8943–8953, https://doi.org/10.1063/1.478813.
[143] M. Álvarez-Moreno, C. de Graaf, N. López, F. Maseras, J.M. Poblet, C. Bo, Managing the computational chemistry big data problem: the ioChem-BD platform, J. Chem. Inf. Model. 55 (1) (2015) 95–103, https://doi.org/10.1021/ci500593j.
[144] D. Van Der Spoel, E. Lindahl, B. Hess, G. Groenhof, A.E. Mark, H.J.C. Berendsen, GROMACS: fast, flexible, and free, J. Comput. Chem. 26 (16) (2005) 1701–1718, https://doi.org/10.1002/jcc.20291.
[145] J. Wang, P. Cieplak, P.A. Kollman, How well does a restrained electrostatic potential (RESP) model perform in calculating conformational energies of organic and biological molecules? J. Comput. Chem. 21 (12) (2000) 1049–1074, https://doi.org/10.1002/1096-987X(200009)21:12<1049::AID-JCC3>3.0.CO;2-F.
[146] A. Chaumont, G. Wipff, Ion aggregation in concentrated aqueous and methanol solutions of polyoxometallates Keggin anions: the effect of counterions investigated by molecular dynamics simulations, Phys. Chem. Chem. Phys. 10 (46) (2008) 6940–6953, https://doi.org/10.1039/B810440A.
[147] X. López, C. Nieto-Draghi, C. Bo, J.B. Avalos, J.M. Poblet, Polyoxometalates in solution: molecular dynamics simulations on the α-$PW_{12}O_{40}^{3-}$ Keggin anion in aqueous media, J. Phys. Chem. A 109 (6) (2005) 1216–1222, https://doi.org/10.1021/jp046862u.
[148] W.L. Jorgensen, J. Chandrasekhar, J.D. Madura, R.W. Impey, M.L. Klein, Development of an improved four-site water model for biomolecular simulations: tip4p-ew, J. Chem. Phys. 79 (1983) 926–935.
[149] M.J. Frisch, G.W. Trucks, H.B. Schlegel, G.E. Scuseria, M.A. Robb, J. R. Cheeseman, G. Scalmani, V. Barone, G.A. Petersson, H. Nakatsuji, X. Li, M. Caricato, A.V. Marenich, J. Bloino, B.G. Janesko, R. Gomperts, B. Mennucci, H. P. Hratchian, J.V. Ortiz, A.F. Izmaylov, J.L. Sonnenberg, F. Ding Williams, F. Lipparini, F. Egidi, J. Goings, B. Peng, A. Petrone, T. Henderson, D. Ranasinghe, V.G. Zakrzewski, J. Gao, N. Rega, G. Zheng, W. Liang, M. Hada, M. Ehara, K. Toyota, R. Fukuda, J. Hasegawa, M. Ishida, T. Nakajima, Y. Honda, O. Kitao, H. Nakai, T. Vreven, K. Throssell, J.A. Montgomery Jr., J.E. Peralta, F. Ogliaro, M. J. Bearpark, J.J. Heyd, E.N. Brothers, K.N. Kudin, V.N. Staroverov, T.A. Keith, R. Kobayashi, J. Normand, K. Raghavachari, A.P. Rendell, J.C. Burant, S. S. Iyengar, J. Tomasi, M. Cossi, J.M. Millam, M. Klene, C. Adamo, R. Cammi, J. W. Ochterski, R.L. Martin, K. Morokuma, O. Farkas, J.B. Foresman, D.J. Fox, Gaussian, Inc., Wallingford CT, 2016.